Dynamic response of steel-concrete composite bridges loaded by high-speed train

Article *in* STRUCTURAL ENGINEERING AND MECHANICS · April 2017

DOI: 10.12989/sem.2017.62.2.179

CITATIONS
19

READS
512

1 author:

Monika Podworna
Wrocław University of Science and Technology
43 PUBLICATIONS **197** CITATIONS

SEE PROFILE

Structural Engineering and Mechanics, *Vol. 62, No. 2 (2017) 179-196*
DOI: https://doi.org/10.12989/sem.2017.62.2.179

Dynamic response of steel-concrete composite bridges loaded by high-speed train

Monika Podworna*

Faculty of Civil Engineering, Wroclaw University of Technology, 27 Wyspianskiego Street, Wroclaw, PL 50370, Poland

(Received December 4, 2015, Revised December 17, 2016, Accepted January 5, 2017)

Abstract. The paper focuses on dynamic analyses of a series of simply-supported symmetric composite steel-concrete bridges loaded by an ICE-3 train moving at high speeds up to 300 km/h. The series includes five bridges with span lengths ranging from 15 m to 27 m, with repeatable geometry of the superstructures. The objects, designed according to Polish standards valid from 1980s to 2010, are modelled on the bridges serviced on the Central Main Line in Poland since 1980s. The advanced, two-dimensional, physically nonlinear model of the bridge-track structure-high-speed train system takes into account unilateral nonlinear wheel-rail contact according to Hertz's theory and random vertical track irregularities equal for both rails. The analyses are focused on the influence of random track irregularities on dynamic response of composite steel-concrete bridges loaded by an ICE-3 train. It has been pointed out that certain restrictions on the train speed and on vertical track irregularities should be imposed.

Keywords: random vertical track irregularities; composite steel-concrete bridge; ICE-3 train; unilateral nonlinear wheel-rail contact; dynamic analysis; Monte-Carlo method

1. Introduction

On the Central Main Line in Poland, there are serviced composite steel-concrete (SC) beam bridges with simply supported spans, separate for each track, with the span length ranging from 15 m to 27 m. The bridges were designed according to Polish standards, in 1980s (PN-82/S-10052 1982, PN-85/S-10030 1985). With regard to the increase of train speed up to 300 km/h planned on this line, it is necessary to predict the behaviour of these objects in the new service conditions. For this purpose, a series of five simply supported composite steel-concrete bridges (SCB) with span lengths ranging from 15 m to 27 m and with repeatable geometry of the superstructures has been designed. The bridges were designed according to Polish standards valid from 1980s to 2010, and are modelled on the bridges serviced on the Central Main Line in Poland since 1980s (Podworna and Klasztorny 2014a).

In this study, an advanced 2D (two-dimensional) physically nonlinear model of the bridge-track structure-high-speed train system, developed by Podworna and Klasztorny (2014b) and cited in a concise form in this contribution, is applied. The model incorporates unilateral nonlinear wheel-rail contact according to Hertz's theory and random vertical track irregularities equal for both rails. The numerical analyses, focused on the influence of random track irregularities on the dynamic response of the structures due to a modern ICE-3 high-speed train, are performed using the computer code worked out in (Podworna and Klasztorny 2014c).

Bridges loaded by high-speed trains should fulfil the serviceability limit state criterion expressed in terms of the vertical deflection of the bridge superstructure, the ultimate limit state criterion with fatigue taken into consideration, the traffic safety criterion expressed in terms of the vertical acceleration of the bridge platform and the passenger comfort criterion expressed in terms of the vertical acceleration of a rail-vehicle body (PN-EN1990 2004). To date, each railway bridge is designed individually.

Vertical track irregularities are considered to be one of the main factors affecting the dynamic response of the bridge / ballasted track structure / high-speed train system (BTT). The irregularities result from track construction technology, periodic maintenance actions, soil settlement and other factors. Experimental measurements and/or modelling of track irregularities are considered in numerous papers, e.g., Antolin *et al.* (2013), Au *et al.* (2002), Guo *et al.* (2012), Lei *et al.* (2002), Rocha *et al.* (2014), Wiriyachai *et al.* (1982), Zhang *et al.* (2008). A common model of railway track roughness vertical profiles is a stationary and ergodic Gaussian process in space. The profile is characterized by a one-sided power spectral density function (PSD). In this study, the PSD function cited in (Au *et al.* 2002, Fryba 1996) corresponding to line grades LG = 4, 5, 6 defined by the Federal Railroad Administration (FRA), USA, is applied.

The dynamic response of railway bridges subjected to high-speed trains has been an important research problem over last decade. The most important contributions are those listed below.

Au *et al.* (2002) develop a 2D vibration study on a railway cable-stayed bridge under a moving train, taking

*Corresponding author, Ph.D.
E-mail: monika.podworna@pwr.edu.pl

ISSN: 2092-7614 (Print), 2092-7622 (Online)

into account random rail irregularities. The main girder of the bridge is modelled using 6 degrees-of-freedom (DOF) Euler beam finite elements. Double-sided constraints between the unsprung masses of the wheel sets and the rails are assumed. The track structure is neglected. Sample vertical profiles of random rail roughness, considered as stationary and ergodic processes in space, are generated using the empirical formula for PSD function with the parameters corresponding to the USA quality classes 1-6.

Zhang *et al.* (2008) analyse, both theoretically and experimentally, the dynamic interaction between the Pioneer Train and the Gouhe Bridge composed of 28 repeatable spans. Each span is a 24 m - span prestressed concrete box girder. The measured track irregularities are used. The 3D multi-body model of a rail-vehicle with four or six wheel-sets is developed. The bridge is modelled spatially with the use of the finite element method (FEM), assuming Rayleigh damping and no relative displacement between the track and the bridge deck. The movement of a wheel set is a function of the bridge deck movement, the random track irregularity and the sinusoidal hunting movement. The specified train velocities are 150-270 km/h.

Guo *et al.* (2012) develop a 3D model of a coupled train-bridge system. Each vehicle is reflected by a linear 27 DOF multi-body system. For the bridge subsystem a linear 3D rail-ballast-beam finite element model was created. Random track irregularities are sampled with the German high-speed track spectra, whereas the wheel hunting is simulated by a sinusoidal function with a random phase. The Sesia viaduct (a composite railway bridge with seven simply supported spans of 46 m) under an ETR500Y train is analysed as a case study, using the modal superposition method.

Antolin *et al.* (2013) develop a 3D train-bridge model taking into account nonlinear wheel-rail contact forces. The multi-body linear model for vehicles and the FEM model for the bridge are formulated. Four wheel-rail interaction models are formulated and compared, i.e., (1) double-sided constraints between a rigid wheel set and the track, (2) uncoupled method, (3) a linear contact model in which lateral relative displacements between rails and wheels are allowed, assuming biconic wheel and rail profiles and linear Kalker theory for tangential contact, (4) a nonlinear model in which realistic wheel and rail profiles, Hertz's nonlinear theory for normal contact and Kalker's nonlinear theory for tangential contact are applied. No separation between wheels and rails is assumed. The track has no independent DOFs. The case study concerns the Gouhe Bridge traversed by the Pioneer Train. The methodology was implemented within FE code Abaqus.

Rocha *et al.* (2014) present a probabilistic methodology for the safety assessment of short span railway bridges under high-speed trains, taking into account track irregularities. The main purpose is to create a procedure that allows identifying the critical train speeds and assessing the safety of the train-bridge system. The composite steel-concrete Canelas Bridge, composed of six simply supported spans of 12 m each and loaded by a TGV double train, is considered as a case study. The linear 2D model was developed with separate displacements for the rail sleepers and the bridge. In total, 23 random variables in reference to the track, bridge and train are taken into account.

Fryba (2001) presents prediction of the forced resonances in single-span single-track railway bridges. The bridge is modelled viscoelastically as an Euler beam, while the train is mapped by a stream of moving forces of the cyclic structure. The author analyses a series of steel-concrete bridges using Galerkin's method.

Cheng *et al.* (2001) examine a 2D linear model of the bridge / track / moving train system incorporating a finite element in the form of two Euler beams connected with the viscoelastic layer and loaded by moving double-mass oscillators.

Song and Choi (2002) present numerical studies of the double-track bridge / moving TGV train system. The authors consider continuous beam bridges using 6 DOF beam finite elements for discretization, including two boundary torsional angles, and took into account the Jacobs bogies. The explicit form of the linear matrix equation of motion was applied.

Podworna (2005a-b) develops a 2D theory of modelling BTT systems. The bridge superstructure is modelled as a step-wise prismatic viscoelastic Timoshenko beam. The rails are mapped by a continuous viscoelastic prismatic Euler beam. Fasteners and ballast-bed are physically nonlinear. The track bed (subsoil) is reflected by a set of equidistant single mass viscoelastic oscillators. The train is composed of vehicles each modelled by the 6DOF Matsuura system.

Lu *et al.* (2009) adopt the vehicle-bridge interaction element in non-stationary random vibration analysis of vehicle/bridge systems. This element condenses DOFs of the vehicle and the bridge using the Newmark integration scheme. The bridge is reflected by a prismatic beam discretised with Euler beam finite elements. The train is composed of a number of vehicles, each reflected by the 6 DOF Matsuura four-axle model.

Doménech *et al*. (2014) compare two approaches to analysis of bridge response under the train moving with high speed. The first one is coupled vehicle-bridge analysis for several vehicle models, and the second one is considering an additional amount of damping which depends on the bridge span. The authors claim that in certain cases the additional damping method overestimates the interaction benefit and this can lead to a non-conservative prediction of bridge response with regard to the acceleration serviceability limit states.

Summing up, hitherto theoretical studies on the effect of random vertical track irregularities on vibrations of railway bridges loaded by high-speed trains were performed on 2D/3D simplified models of BTT systems. Researchers made various assumptions, applied various methodologies and analysed bridges of different types. The influence of random track irregularities on the dynamic response of beam composite bridges loaded by a high-speed train, taking into account nonlinear properties of the track structure and wheel-rail micro-detachment, has not been analysed yet.

In this study, random track irregularities, the track structure with nonlinear properties and nonlinear wheel-rail contact with the possibility of contact loss at wheels are

taken into consideration.

2. Description of SCB bridges

The SCB series of railway bridges was designed according to Polish standards (PN-82/S-10052 1982, PN-85/S-10030 1985), under the following main assumptions:

- bridges are single-span and simply-supported and are located on the main railways;
- the axis of the unloaded railway track is rectilinear and horizontal;
- bridges have a composite steel-concrete superstructure and have separate spans for each track.

The detailed description of the design process is presented in (Podworna and Klasztorny 2014a). The series includes five objects of codes and basic geometric parameters listed in Table 1, where L [m] - theoretical span length (a distance between support pivots), L_T [m] - total length of the main girders, H [m] - structural height. The series is modelled on the bridges serviced on the Central Main Line in Poland since 1980s. The main technical data of SCB objects are as follows:

- the superstructure is composed of four steel I-beams and a reinforced concrete slab platform;
- main steel beams are of depth of 770-1370 mm, made of S235W steel, their bottom flanges are reinforced with one flat 0.6 L long;
- the main beams are reinforced vertically and horizontally in pairs, with L100×100×10 steel angles using welding;
- 10 mm thick vertical ribs, welded to the I-beam webs and positioned at intervals of 1500 mm;
- a discrete connection of the main steel beams with the RC platform is executed with the use of steel anchors of dimensions ϕ12 mm, l=170 mm;
- the RC platform plate is 250 mm thick, made of C30/37 concrete and reinforced with AII/18G2-B steel;
- a levelling concrete layer of 0-40 mm thickness is characterized by a 2% two-sided transverse slope;
- concrete kerbs of the platform are 250 mm high; there are applied 1 cm wide vertical dilatations at intervals of 1.50 m;
- RC bridgehead foundations are used;
- approach slabs, used to minimize the threshold effect, are supported on the unmovable steel pivot bearings, made of C30/37 concrete and reinforced with AII/18G2-B steel; their dimensions are 5.00 m - total length, 4.00 m - width, 20 cm - thickness, 2% two-sided transverse slope;
- the track structure is composed of: continuously welded 60E1 (UIC-60) operating rails, 60E1 (UIC-60) side rails of length covering the bridge span and the approach slabs, prestressed concrete sleepers, first class crushed stone ballast to the depth of 35 cm under the sleepers, Vossloh 300-1fasteners of the main and side rails;
- a single service sidewalks is used;
- the bridge is supported on movable steel pivot bearings at the train entrance side and on fixed steel pivot bearings at the opposite side.

Table 1 Codes, basic geometric parameters and limit deflections of bridges forming SCB bridge series

Bridge code	SCB-15	SCB-18	SCB-21	SCB-24	SCB-27
L [m]	15.00	18.00	21.00	24.00	27.00
L_T [m]	15.80	18.80	21.80	24.80	27.80
H [m]	1.82	1.97	2.12	2.27	2.42
W_u=L/600 [mm]	25	30	35	40	45

The cross-section of the selected SCB bridge at midspan, with GFRP composite side walls, is shown in Fig. 1. The cross-sections of SCB-18, SCB-21, SCB-24, SCB-27 bridges are analogous; only dimensions of the webs and bottom flanges of the main beams as well as the vertical brackets change respectively.

The longitudinal section, including selected the SCB bridge and the transient zone part, is depicted in Fig. 2. There can be observed the ribs stiffening the webs of the steel beams at 1500 mm intervals, the support ribs located every 200 mm, a 600 mm long bearing plate, flats reinforcing the bottom flanges of the length of 0.6 L=9000 mm, kerbstones with 1 cm dilatations every 1500 mm, CFRP composite protective walls with 1 cm dilatations every 1500 mm, an approach slab of the total length of 5000 mm.

Table 2 collects the values of the basic parameters of SCB bridges used in the numerical modelling of BTT systems. The following quantities are included:

- $W_b(0.5L), W_t(0.5L)$ - bending indices the bottom and top fibres of the equivalent steel cross-section of the bridge superstructure, at midspan;
- $EI(0.5L)$ - flexural stiffness of the equivalent steel cross-section of the bridge superstructure, at midspan;
- $m(0.5L)$ - mass per unit length of the equivalent steel cross-section of the bridge superstructure, at midspan (with isolation layer, levelling concrete, kerbs, covers, sidewalk, joints, ribs, brackets taken into account);
- $EI(0), m(0)$ - stiffness and mass parameters of the equivalent steel cross-section of the bridge superstructure, at the supports;
- γ - damping ratio of the bridge superstructure,
- $f_l = 1$ Hz, $f_u = 500$ Hz - vibration frequency range in which the bridge superstructure damping is approximately constant (the Rayleigh model of damping).

Mass of the ballast layer was discretised as a set of point masses M_b = 2900 kg, spaced by d, located under sleepers. In the bridge-approach slabs zone, the point masses M_b were added to respective nodal points of beam finite elements.

The subsequent physical parameters occurring in the numerical modelling of BTT systems have the following values (Podworna and Klasztorny 2014a): $\rho_b = 2000$ kg/m^3, $m_r, m_{sr} = 120$ kg/m, $M_s = 366$ kg, $m_b = 4833$ kg/m, $m_a = 2000$ kg/m, $L_a = 4.80$ m, $2D = 204$ m, $d = 0.60$ m, where: ρ_b- ballast density,

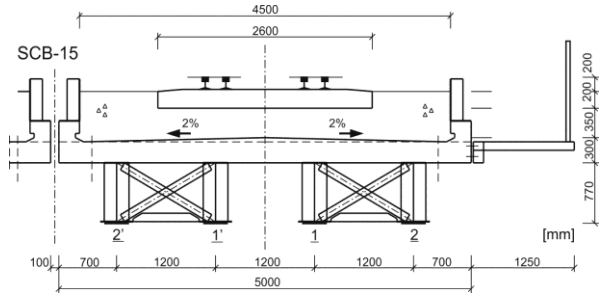

Fig. 1 Cross-section of symmetric SCB-15 bridge, with composite side walls, at midspan

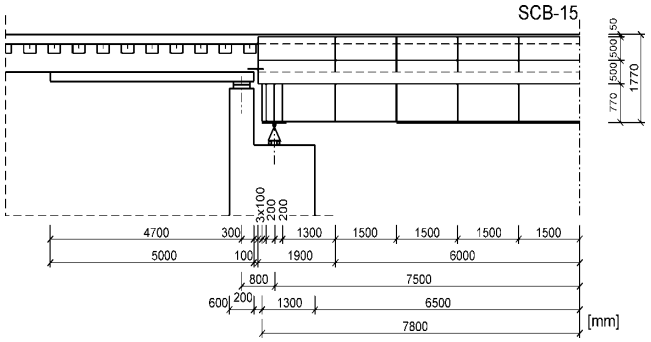

Fig. 2 Longitudinal section of symmetric SCB bridge and approach slab zone

m_r - mass of the main rails per unit length, m_{sr} - mass of the side rails per unit length, M_s - mass of one sleeper and two fasteners, m_b - mass of the ballast per unit length, m_a - mass of the approach slab per unit length, L_a - length of the approach slab, D - half of the deformable track section before the left approach slab and after the right approach slab, d - sleeper spacing.

3. Modelling of wheel - rail contact stiffness and random vertical track irregularities

Advanced modelling of the wheel-rail contact stiffness according to the Hertz theory is presented by Lei and Noda (2002). This contact is considered as two elastic contact cylinders perpendicular to each other. The relative vertical shortening between the wheel and the rail is calculated from the conventional Hertz formula

$$u_H = d_H R_1^{2/3} \tag{1}$$

where: u_H - vertical shortening, $d_H = 1/k_H$ - contact compliance, k_H - contact stiffness, $R_1 = 0.5R$ - half of the interaction force per a wheel set. The average value of contact stiffness coefficient $k_H = 0.216 \times 10^8 \left[\mathrm{N}^{2/3}/\mathrm{m}\right]$ per one wheel.

In reference to a 2D model of the BTT system, only the vertical profile of random track irregularities, i.e. the mean vertical elevation of two rails, is taken into consideration. Short wavelength corrugation irregularities in the rail are neglected. A stationary and ergodic Gaussian process in space is characterised by a one-sided PSD function $S_{rr}(\Omega)$, with $\Omega = 2\pi/L_r$ [rad/m] as a distance frequency, and L_r as wavelength. This function is defined by the formula determined by FRA (Fryba 1996)

$$S_{rr}(\Omega) = kA\frac{\Omega_c^2}{\left(\Omega^2 + \Omega_c^2\right)\Omega^2} \quad \left[\frac{\mathrm{mm}^2 \cdot \mathrm{m}}{\mathrm{rad}}\right] \tag{2}$$

where $k = 0.25$, $\Omega_c = 0.8245$ [rad/m]. Coefficient A [mm^2×rad/m] is specified for line grades 1-6. Only better lines of grades LG=4 (A = 53.76), LG=5 (A = 20.95), and LG=6 (A=3.39) are considered in this study.

Random samples of a track irregularity vertical profile are generated with the Monte-Carlo method (Fryba 1996)

$$r(x) = 2\sum_{i=1}^{N_r}\sqrt{S_{rr}(\Omega_\mathrm{i})\cdot\Delta\Omega}\cos(\Omega_i x + \varphi_i) \quad [\mathrm{mm}] \tag{3}$$

Table 2 Main parameters of SCB bridges

Parameter	Unit	SCB-15	SCB-18	SCB-21	SCB-24	SCB-27
L	m	15.00	18.00	21.00	24.00	27.00
$W_b(0.5L)$	m^3	0.092242	0.118366	0.153232	0.191603	0.232258
$W_t(0.5L)$	m^3	0.153681	0.196170	0.250882	0.307435	0.374040
$EI(0.5L)$	Nm^2	13.897×10^9	20.824×10^9	31.710×10^9	45.395×10^9	63.917×10^9
$EI(0)$	Nm^2	10.289×10^9	15.561×10^9	23.956×10^9	34.622×10^9	49.391×10^9
$m(0.5L)$	kg/m	5300	5470	5660	5850	6020
$m(0)$	kg/m	5050	5210	5380	5550	5710
	-	0.01125	0.0075	0.005	0.005	0.005

where:

x - abscissa measured along the track;

$\Omega_i = \Omega_{\min} + (\mathrm{i} - 0.5)\Delta\Omega$ - discrete distance frequency;

φ_i - random phase angle uniformly distributed over the $[0, 2\pi]$ [rad] interval and independent for $i = 1,2, \ldots, N_r$;

$\Delta\Omega = \frac{1}{\mathrm{N_r}}(\Omega_{\max} - \Omega_{\min})$ - distance frequency increment;

N_r - total number of distance frequency increments in the interval $[\Omega_{\min}, \Omega_{\max}]$;

$\Omega_{\min} = \frac{2\pi}{L_{r,\max}}$, $\Omega_{\max} = \frac{2\pi}{L_{r,\min}}$ - lower and upper limits of the distance frequency;

$L_{r,\min}, L_{r,\max}$ - lower and upper limits of the wavelength.

The testing simulations of random vertical track irregularities were performed using a corresponding computer code in Delphi by Podworna and Klasztorny (2014c). Taking into account the experimental data available in (Au *et al.* 2002, Lei *et al.* 2002, Song *et al.* 2008, Fryba 1996) and the testing simulations, the values of $L_{r,\min} = 0.10$ m, $L_{r,\max} = 70.00$ m, $N_r = 100$ are assumed.

According to PN-EN13848-5 (2010), track irregularity profiles are characterized by the peak values of track irregularities or by the standard deviation calculated over the track section of typically 200 m length. For high-speed lines the alert limit (AL) peak value interval of track irregularities, in reference to longitudinal level, is $r_{\mathrm{peak}} \in [12\ \mathrm{mm}, 18\ \mathrm{mm}]$ for the wavelength range $25\ \mathrm{m} < \lambda \leq 70\ \mathrm{m}$ (*see* Table B.3 in PN-EN13848-5

(2010). The alert limit refers to the value which if exceeded, requires that the track geometry condition is analysed and considered in the regularly planned maintenance operation. Based on the test simulations, the following values are obtained: $r_{\text{peak}} \in [13\text{ mm}, 17\text{ mm}]$ for LG = 4, $r_{\text{peak}} \in [8.1\text{ mm}, 10.6\text{ mm}]$ for LG = 5, and $r_{\text{peak}} \in [3.3\text{ mm}, 4.3\text{ mm}]$ for LG = 6. The peak value interval for LG = 4 matches the AL peak value interval of track irregularities specified in PN-EN13848-5 (2010).

In this study, vibration simulations of BTT systems are conducted for the line grades LG = 4, 5, 6 for research purposes.

4. Output functions, output quantities and design quantities

The following output functions are introduced:

$w(x,t)$ - vertical deflection of the bridge superstructure;

$\sigma(x,t)$ - longitudinal normal stress in the bottom fibres of the main beams;

$a_p(x,t)$ - vertical acceleration of the reinforced-concrete platform;

where t - time variable. The abscissa $x = 0$ at the left support of the bridge.

The following output quantities are defined:

$w(0.5L,t)$ - vertical deflection of the bridge superstructure at midspan [mm];

$\sigma(0.5L,t)$ - longitudinal normal stress in the bottom fibres of the main beams at midspan [MPa];

$a_{\text{p}}(0.5L,t)$ - vertical acceleration of the reinforced-concrete platform at midspan [m/s^2];

$R_{ki}(t),\ k = 1,2,3,4,\ i = 1,2,\dots,N_v$ - dynamic pressure force of a wheel set onto rails [kN] (k - number of a wheel set, i - number of a vehicle, N_v - number of rail-vehicles);

$a_{bi\alpha}(t),\ i = 1,2,\dots,N_v,\ \alpha = f,r$ - vertical acceleration of a vehicle body at the pivots over the front ($\alpha = f$) and rear ($\alpha = r$) bogies [m/s^2].

The following design quantities are defined

$$\begin{gathered} \text{w}_{\max} = \max_t\ w(0.5L,t) \\ \sigma_{\max} = \max_t\ \sigma(0.5L,t) \\ a_{\text{p,max}} = \max_t |a_p(0.5L,t)| \\ R_{\min} = \min_t\ \{R_{ki}(t)\},\ k = 1,2,3,4,\ i = 1,2,\dots,N_v \\ a_{\text{b,max}} = \max_t \{\,|a_{bi\alpha}(t)|\,\},\ i = 1,2,\dots,N_v,\ \alpha = f,r \end{gathered} \tag{4}$$

Impact factors in the vertical deflection and in the longitudinal normal stress in the bottom fibres of the main beams, both at midspan, are calculated from well-known classic formulae, i.e.

$$\begin{aligned} \varphi_w(0.5L) &= \frac{\max_t\ w(0.5L,t)}{\max_t w_s(0.5L,t)} \\ \varphi_\sigma(0.5L) &= \frac{\max_t\ \sigma(0.5L,t)}{\max_t \sigma_s(0.5L,t)} \end{aligned} \tag{5}$$

where:

$w(0.5L,t), \sigma(0.5L,t)$ - dynamic vertical deflection and dynamic longitudinal normal stress, respectively, simulated with or without random track irregularities for the selected resonant and extra-resonant train speeds;

$w_s(0.5L,t), \sigma_s(0.5L,t)$ - quasi-static vertical deflection and quasi-static longitudinal normal stress, respectively, simulated for the train speed $v =$ 30 km/h and for the smooth track.

5. Design criteria for bridges located on high-speed lines

According to PN-EN1990 (2004), composite steel-concrete bridges loaded by high-speed trains should fulfil the serviceability limit state criterion expressed in terms of the vertical deflection of the bridge superstructure, the ultimate limit state criterion with fatigue taken into consideration, the traffic safety criterion expressed in terms of the vertical acceleration of the bridge platform and the passenger comfort criterion expressed in terms of the vertical acceleration of a rail-vehicle body.

The serviceability limit state criterion, expressed in terms of the vertical deflection of the bridge superstructure loaded by a high-speed train, has the following form

$$w_{\max} \le w_{\text{u}} \tag{6}$$

where: $w_{\max}$ - maximum value of the vertical deflection of the bridge superstructure at midspan (Eq. $(4)_1$), $w_{\text{u}} = L/600$ is the limit value for the vertical deflection (PN-EN1990 2004). This is the limit state for traffic safety, but is not related to passenger comfort and is not the most restrictive condition to be fulfilled by the vertical deflection.

In this study, the ultimate limit state criterion, with fatigue taken into consideration, refers to the longitudinal normal stresses in the bottom fibres of the main steel beams at midspan. This criterion can be formulated as Podworna and Klasztorny (2014c)

$$\sigma_f(0.5L) = \sigma_{gk}(0.5L) + \sigma_m(0.5L) + \zeta\sigma_a(0.5L) \le \sigma_{\text{u}} \tag{7}$$

where:

$\sigma_f(0.5L)$ - equivalent normal stress including high-cycle fatigue;

$\sigma_{gk}(0.5L)$ - normal stress due to characteristic self-weight of the bridge;

$\sigma_m(0.5L)$ - average normal stress corresponding to the quasi-steady-state vibrations;

$\sigma_a(0.5L)$ - amplitude of normal stress corresponding to the quasi-steady-state vibrations;

ζ - high-cycle fatigue factor;

σ_{u} - limit value for normal stress.

Eq. (7) is obtained from the Schmidt graph approximated with an open polygon, assuming a constant safety margin. For S235W structural steel, the high-cycle fatigue factor is $\zeta = 2.35$, and the limit value for normal stress equals $\sigma_{\text{u}} = f_{yk}/n_s = 157$ MPa , where $f_{yk} =$ 235 MPa - yield strength, $n_s = 1.5$ - safety margin (safety coefficient) (Podworna and Klasztorny 2014c).

The traffic safety criterion (the serviceability limit state for prevention of track instability) is formulated in reference to the maximum peak of the low-pass filtered vertical acceleration of the bridge span at the midspan and takes the following form (Podworna and Klasztorny 2014)

$$a_{p.\max} \leq a_{p,u} \tag{8}$$

where:

$a_{p,\max}$ - maximum peak of the low-pass filtered vertical acceleration of the bridge span at the midspan (Eq. $(4)_3$);

$a_{p,u} = 3.5$ m/s^2 - recommended maximum value of the low-pass filtered vertical acceleration of a railway bridge span at the midspan for a ballasted track, including vibrations of frequencies not exceeding:

a) 30 Hz,
b) 1.5 - times the fundamental frequency of a bridge span,
c) the 3rd natural frequency of a bridge span.

This standard criterion the author interprets as a requirement of low-pass filtering of the acceleration time-histories. Due to the non-linear physical model of the bridge - track - high-speed train, the case a) has been selected, although the case b) leads to an even greater reduction in frequency. The case c) results in limitation of greater than 30 Hz. In the remaining standard design conditions, the full range of frequencies resulting from the accepted model of the bridge - track - high-speed train discrete system has been taken into consideration.

As it will be shown in further considerations, the numerical modelling of SCB bridges results in a non-linear discrete system with a large number of DOFs and high frequency oscillations. Thus, low pass filtering of the platform acceleration signal, $a_p(0.5L, t)$, is required. In this study, the low pass ideal filter, available in Hyper Graph 12.0 code, is used. The maximum value of the filtered platform acceleration at midspan is denoted with the symbol $a_{p,\max}^{\mathrm{LPF}}$.

The passenger comfort criterion, expressed in terms of the vertical acceleration of a rail-vehicle body, takes the following form (Podworna and Klasztorny 2014c)

$$a_{b,\max} \leq a_{b,\mathrm{u}} \quad , \quad i = 1, 2, \ldots, N_v \tag{9}$$

where:

$a_{b,\max}$ - maximum vertical acceleration registered at the vehicle body pivots (suspension points) (Eq. $(4)_5$);

$a_{b,u}$ - limit value of vertical acceleration inside the coach during the travel, specified in PN-EN1990 (2004). The value $a_{b,u}$ is equal to 1.0, 1.3, 2.0 for the very good, good and acceptable level of comfort, respectively.

6. Description of modelling of BTT systems

Advanced physical and mathematical 2D modelling of BTT systems was developed by Podworna and Klasztorny (2014b). In this study, the BTT modelling presented in this reference is cited in a concise form. In the modelling, the following main assumptions are adopted:

- There is considered a finitely long deformable track, with continuously welded rails, including the out-of-transition zones, the transition zones and the bridge zone.
- Random vertical track irregularities result from construction and maintenance of the track as well as from settlement of the ballast and subgrade.
- Operating and side rails are viscoelastic prismatic beams deformable in flexure. Rail-sleeper fasteners are viscoelastic elements with physically non-linear elastic characteristic. The sleepers vibrate vertically and are modelled as concentrated masses.
- The ballast is modelled as a set of vertical viscoelastic constraints with physically non-linear elastic characteristic. This model includes possible micro detachment of a sleeper from the ballast. The lumped ballast model is used.
- The track bed (subsoil) is a linearly viscoelastic layer modelled discretely.
- The approach slabs are modelled as viscoelastic prismatic beams deformable in flexure.
- The bridge superstructure is reflected by a simply supported viscoelastic stepwise prismatic beam, deformable in flexure, symmetrical relative to the bridge midspan.
- Rail-vehicles form a high-speed ICE-3 German train. Possible wheel-rail microseparations and impacts of the moving wheel sets onto the main rails are taken into consideration.
- Train velocity v is constant and ranges from 30 to 300 km/h. A velocity of 30 km/h is treated as relevant to the quasi-static passage of the train.
- Vibrations of the BTT system are physically nonlinear and geometrically linear.

A BTT system is composed of the following inertial subsystems (Figs. 3, 4): BS - bridge superstructure, LAS - left approach slab, RAS - right approach slab, LB - left ballast-bed, RB - right ballast-bed, SL -sleepers, OR - operating rails, SR -side rails, RV$i, i = 1,2, \ldots, N_v$ - railway vehicles. These subsystems are subjected to relevant subsets of the vertical interaction forces carried by elastic/viscoelastic physically linear/nonlinear constraints. Symbols used in Figs. 3, 4 have the following meanings:

VVRZ (Vehicle Vibration Registration Zone) - zone of $(2D + L_{\mathrm{o}})$ length, in which the following quantities are registered: the dynamic pressure forces of the wheel sets onto the main rails and the vertical accelerations of vehicle bodies at the pivots;

BVRZ (Bridge Vibration Registration Zone) - zone of $(2D + L_{\mathrm{o}} + L_v)$ length; when the train head is in this zone, the following quantities are registered at midspan: the vertical deflection of the bridge superstructure, the longitudinal normal stress in the bottom fibres of the main beams, the vertical acceleration of the bridge platform;

$L_{\mathrm{o}} = (L + 2L_a + 2d)$ - bridge span length plus length of approach slabs plus two sleeper intervals;

L_v - train set length;

v - operating velocity (horizontal service velocity of the train);

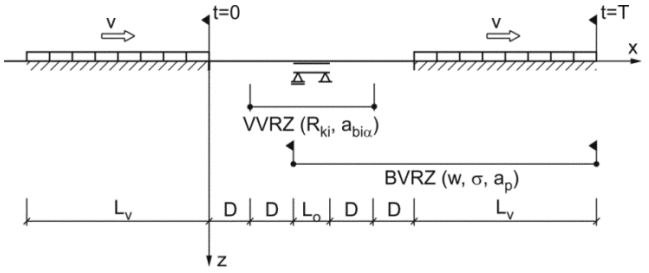

Fig. 3 Schematic diagram of BTT system at time t=0 and t=T

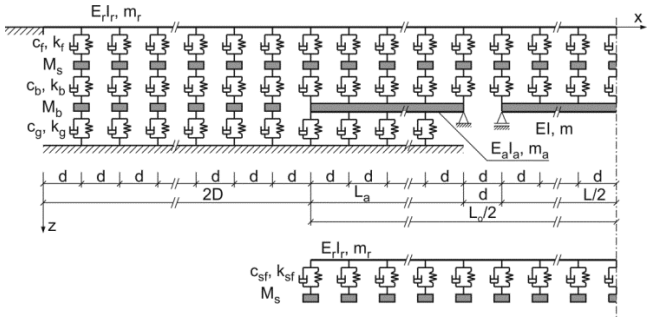

Fig. 4 Physical model of symmetric bridge / track structure subsystem (left part)

x, z - coordinates of the planar system;

$T = (4D + L_o + L_v)/v$ - dynamic process duration time;

$EI(x), m$(x) - flexural stiffness and mass per unit length of the bridge superstructure;

$E_r I_r, m_r$ - flexural stiffness and mass per unit length of the rails;

$E_a I_a, m_a$ - flexural stiffness and mass per unit length of the approach slabs;

$c_f, k_f, c_{sf}, k_{sf}, c_b, k_b, c_g, k_g$ - partly nonlinear damping and stiffness coefficients in reference to the main rails, the side rails, the ballast, and the track subsoil, respectively.

Over the bridge span and the approach slabs, the uniformly distributed ballast mass is added to the bridge superstructure mass and the approach slabs mass, respectively.

A finitely long section of the deformable track is depicted in Fig. 3. The out-of-approach zones have length of 2D. The first D section from the train entering side enters subsequent vehicles into the quasi-stationary random vibration state.

A 2D physical model of the track structure / bridge subsystem is presented in Fig. 4. Constant sleeper spacing d is used to discretize the subsystem. The main rails are fixed at the ends of the finite-long section of the track of length $(4D + L_o)$. The side rails have length of L_o and are fixed to the sleepers viscoelastically. Viscoelastic elements modelling the fasteners and the ballast incorporate physically nonlinear elastic constraints. Discretization of the beams modelling the operating and side rails, the approach slabs and the bridge superstructure uses classic prismatic beam finite elements deformable in flexure, with 4DOF and length d. Finite element nodes correspond to the positions of the sleepers at intervals d. Step-wise changes in the parameters of the bridge superstructure are in the relevant finite element nodes - Podworna and Klasztorny (2014b).

A non-linear elastic characteristic of rail fastenings is illustrated in Fig. 5. In the simulations, chart b) should be taken into consideration (the compression induced by the self-weight of the rails is included). The interactive force R_f is positive when the vertical constraints are shortened by the value of u and equals (Podworna and Klasztorny 2014b)

$$R_f(u,\dot{u}) = \begin{cases} k_{f1}u + c_f\dot{u}\ , & -u_{fo} \le u \le u_f - u_{fo} \\ k_{f1}(u_f - u_{fo}) + k_{f2}\left[u - (u_f - u_{fo})\right] + c_f\dot{u}\ , & u > u_f - u_{fo} \\ k_{f1}(-u_{fo}) + k_{f3}(u + u_{fo}) + c_f\dot{u}, & u < -u_{fo} \end{cases} \quad (10)$$

where

$$u_{fo} = \frac{M_r g}{k_{f1}} \quad (11)$$

with $g = 9.81$ m/s^2 - gravity acceleration.

Crushed stone ballast is a linearly elastic layer in compression and does not transmit tension. A non-linear elastic characteristic of the ballast-bed layer is illustrated in Fig. 6. In the simulations, chart b) should be taken into account (the compression resulting from the self-weight of the rails and the sleepers is included). The interactive force R_b is positive when the vertical constraints are shortened by the value of u and equals (Podworna and Klasztorny 2014b)

$$R_b(u,\dot{u}) = \begin{cases} k_{b1}u + c_b\dot{u}\ , & u \ge -u_{bo} \\ k_{b1}(-u_{bo}) + c_b\dot{u}\ , & u < -u_{bo} \end{cases} \quad (12)$$

where

$$u_{bo} = \begin{cases} \dfrac{(2M_r + M_s)g}{k_{b1}}\ , & x \in [2D;\, 2D + L_o] \\ \dfrac{(M_r + M_s)g}{k_{b1}}\ , & x \in [0;\, 4D + L_o]\backslash[2D;\, 2D + L_o] \end{cases} \quad (13)$$

ICE (Inter City Express) high-speed trains were built by Siemens Company in 2000 and 2001 in the total number of 50 trains (Series 1). The ICE-3 is the third generation of the

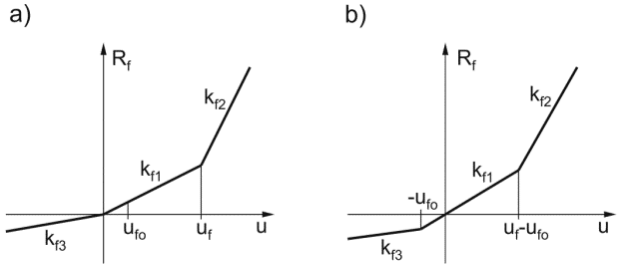

Fig. 5 Elastic characteristic of rail fastenings: (a) before taking into account static compression induced by weight of rails; (b) after taking into account static compression induced by weight of rails

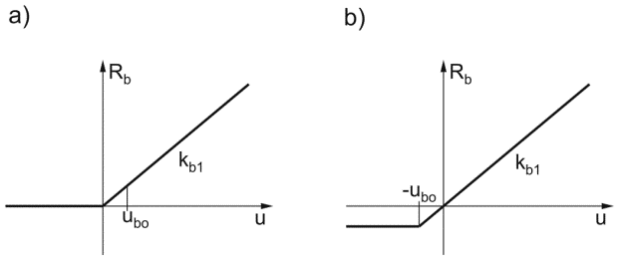

Fig. 6 Elastic characteristic of ballast layer: (a) before taking into account static compression induced by weight of rails and sleepers; (b) after taking into account static compression induced by weight of rails and sleepers

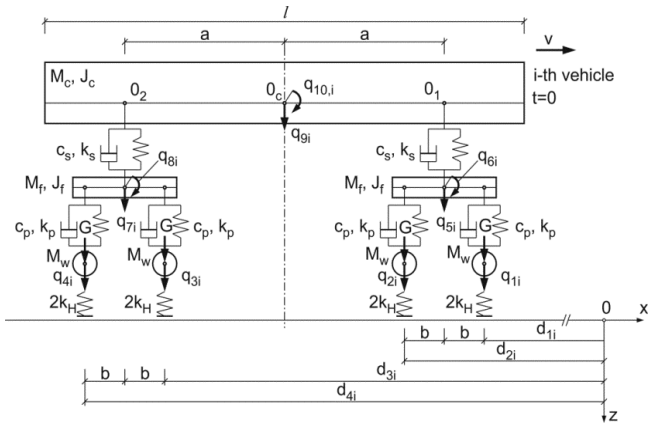

Fig. 7 Enhanced Matsuura model of rail-vehicle and its position at t=0

German high-speed trains. The main difference in comparison to the previous generations is a multiple unit power system. The train has no end power heads as an ICE-1 train, but it has motor bogies located every second car. It results in improved operating parameters. The total weight is distributed evenly across the entire trainset, therefore the axle load is reduced to 16 metric tons. The ICE-3 trainset contains 8 cars. Configuration of the four end cars is usually a mirror reflection of the four front cars, which are set as follows: a power car supported on two SF 500 TDG motor bogies, a transformer car supported on two SF 500 TDG trailer bogies, a converter car supported on two SF 500 TDG motor bogies, an intermediate car supported on two SF 500 TDG trailer bogies. The structure of primary and secondary suspension systems is the same in both bogies. They are equipped with two coil springs and two vertical dampers per axle (one per each axle box) for primary suspension and two air springs and two vertical dampers per bogie for the secondary suspension system. The difference between motor and trailer bogies - besides a motor and transmission - is related to the break system. Powered axles are equipped with two wheel-mounted break discs per wheelset, whereas the non-driven axles have three axle-mounted break discs, in addition (Steimel 2007, http 2010a, http 2010b, http 2010c). The top speed in service is equal to 300 km/h. Based on (Steimel 2007, http 2010a, http 2010b, http 2010c), the parameters corresponding to planar models for power, transformer, converter and intermediate cars are listed by Podworna and Klasztorny (2014c).

The dynamic analyses are conducted for an ICE-3 train using the enhanced Matsuura model of a rail-vehicle (Fig. 7). Each vehicle has two independent two-axle bogies. Matsuura's 2D model of a rail-vehicle is developed via incorporating non-linear one-sided wheel-rail contact springs. Potential detachment of the moving wheels from the rail heads is taken into consideration.

The enhanced Matsuura model of a four-axle rail-vehicle is defined as follows (Fig. 7):

- Wheel sets are modelled as point masses vibrating vertically, each with 1DOF.
- Bogie frames are modelled as rigid disks, each with 2DOF (vertical translation and in-plane rotation).
- The vehicle body is modelled as a rigid disk with 2DOF (vertical translation and in-plane rotation).
- Suspensions of the first and second stage are linear and viscoelastic.
- The first-stage suspension pivots are at the same height as the bogie mass centre. The second-stage suspension pivots are at the same height as the body mass centre.

Masses modelling wheel sets are fitted with one-sided vertical springs reflecting the Hertzian contact and described by Eq. (1).

Each rail-vehicle is a non-linear discrete system with 10DOFs. The nonlinearity results from Eq. (1) and one-sided Hertz contact springs. A detailed description of the rail-vehicle modelling is presented in Podworna and Klasztorny (2014b).

Using the Lagrange equations of the second order results in linear matrix equations of motion of individual subsystems, with the generalized load vectors stored in the implicit form. This formulation leads to equations of motion of the subsystems with constant coefficients. Coupling and physical non-linearity of the subsystems are hidden in the generalized load vectors expressed in terms of the interaction forces.

Transient and quasi-steady-state vibrations of the BTT system are governed by $8 + N_v$ matrix equations of motion, in the following implicit form (Podworna and Klasztorny 2014b)

$$\begin{gathered}
\mathbf{B}\ddot{\mathbf{q}} + \mathbf{C}\dot{\mathbf{q}} + \mathbf{K}\mathbf{q} = \mathbf{F} \\
\mathbf{B}_{la}\ddot{\mathbf{q}}_{la} + \mathbf{C}_{la}\dot{\mathbf{q}}_{la} + \mathbf{K}_{la}\mathbf{q}_{la} = \mathbf{F}_{la} \\
\mathbf{B}_{ra}\ddot{\mathbf{q}}_{ra} + \mathbf{C}_{ra}\dot{\mathbf{q}}_{ra} + \mathbf{K}_{ra}\mathbf{q}_{ra} = \mathbf{F}_{ra} \\
\{\mathbf{M}_b\}\ddot{\mathbf{q}}_{lb} = \mathbf{F}_{lb} \\
\{\mathbf{M}_b\}\ddot{\mathbf{q}}_{rb} = \mathbf{F}_{rb} \\
\{\mathbf{M}_s\}\ddot{\mathbf{q}}_s = \mathbf{R}_f - \mathbf{R}_b \\
\mathbf{B}_r\ddot{\mathbf{q}}_r + \mathbf{C}_r\dot{\mathbf{q}}_r + \mathbf{K}_r\mathbf{q}_r = \mathbf{F}_r \\
\mathbf{B}_{sr}\ddot{\mathbf{q}}_{sr} + \mathbf{C}_{sr}\dot{\mathbf{q}}_{sr} + \mathbf{K}_{sr}\mathbf{q}_{sr} = \mathbf{F}_{sr} \\
\mathbf{B}_i\ddot{\mathbf{q}}_i = \mathbf{F}_i \ , \quad \mathrm{i} = 1, 2, \dots, N_v
\end{gathered} \tag{14}$$

where:

$\mathbf{q}(t)$, $\mathbf{q}_{la}(t)$, $\mathbf{q}_{ra}(t)$, $\mathbf{q}_{lb}(t)$, $\mathbf{q}_{rb}(t)$, $\mathbf{q}_s(t)$, $\mathbf{q}_r(t)$, $\mathbf{q}_{sr}(t)$ - vectors of generalized coordinates in reference to BS, LAS, RAS, LB, RB, SL, OR, SR subsystems, respectively;

$\mathbf{q}_i(t), i = 1,2, \dots, N_v$ - vectors of generalized coordinates for subsequent rail-vehicles;

$\mathbf{B}, \mathbf{C}, \mathbf{K}$ - mass, damping and stiffness matrices for BS subsystem; respectively;

$\mathbf{B}_{la}, \mathbf{C}_{la}, \mathbf{K}_{la}, \mathbf{B}_{ra}, \mathbf{C}_{ra}, \mathbf{K}_{ra}$ - mass, damping and

stiffness matrices for LAS and RAS subsystems, respectively;

$\{\mathbf{M}_b\}$ - mass matrix for LB and RB subsystems;

$\{\mathbf{M}_s\}$ - mass matrix for SL subsystem;

$\mathbf{B}_r, \mathbf{C}_r, \mathbf{K}_r, \mathbf{B}_{sr}, \mathbf{C}_{sr}, \mathbf{K}_{sr}$ - mass, damping and stiffness matrices for OR and SR subsystems, respectively;

$\mathbf{B}_i$ - mass matrix for the i^{th} rail-vehicle;

$\mathbf{R}_f, \mathbf{R}_{sf}$ - vectors of interaction forces transmitted by fasteners in OR and SR subsystems, respectively;

$\mathbf{R}_b$ - vector of interaction forces transmitted by the ballast bed;

$\mathbf{R}_g$ - vector of interaction forces transmitted by the track bed;

$\mathbf{R}_{wi}$ - vector of moving pressure forces of the i^{th} vehicle wheel sets acting on the rails;

$\mathbf{F}(\mathbf{R}_b)$ - generalized load vector in the implicit form, related to BS subsystem;

$\mathbf{F}_{la}(\mathbf{R}_b, \mathbf{R}_g)$, $\mathbf{F}_{ra}(\mathbf{R}_b, \mathbf{R}_g)$ - generalized load vectors in implicit form, related to LAS and RAS subsystems, respectively;

$\mathbf{F}_{lb}(\mathbf{R}_b, \mathbf{R}_g)$, $\mathbf{F}_{rb}(\mathbf{R}_b, \mathbf{R}_g)$ - generalized load vectors in implicit form, related to LB and RB subsystems, respectively;

$\mathbf{F}_r(\mathbf{R}_f, \mathbf{R}_{wi})$, $i = 1,2,\dots,N_v$; $\mathbf{F}_{sr}(\mathbf{R}_{sf})$ - generalized load vectors in implicit form, related to OR and SR subsystems, respectively;

$\mathbf{R}_i = \text{col}\,(R_{1i}R_{2i}\dots R_{10,i})$ - vector of vertical interactions transmitted by the 1st and 2nd stage suspensions of i^{th} vehicle;

$\mathbf{G}$ - generalized load vector reflecting static pressures of the wheel sets onto the rails;

$\mathbf{F}_i(\mathbf{R}_i, \mathbf{G}), i = 1,2,\dots,N_v$ - generalized load vector in implicit form, related to RVi, $i = 1,2,\dots,N_v$ subsystem;

$(\dot{\ }) = d/dt$ - differentiation with respect to time variable t.

Detailed formulae defining matrices and vectors in Eqs. (14) are derived in (Podworna and Klasztorny 2014b). An implicit (recurrent-iterative) algorithm for numerical integration of the matrix equations of motion (14) is also developed in (Podworna and Klasztorny 2014b). The algorithm is based on the Newmark average acceleration method and the linear prediction of the interactions.

The method of physical and numerical modelling of the BTT system enables formulation of the matrix equations of motion of a highly complex physically nonlinear system in a relatively easy way, and reduces the CPU time several times compared to the models in the explicit form. Compared to the state-of-the-art, the 2D physical model of BTT systems developed in (Podworna and Klasztorny 2014b) is the most advanced in the 2D model class.

7. Prediction of forced resonances

A BTT system is physically nonlinear in reference to the ballast layer, rail fastenings, and one-sided non-linear wheel-rail constraints. A geometrically infinite track is mapped approximately via finitely long out-of-approach zones of the track. Based on the preliminary simulations, it is concluded that the BT (bridge / track structure) subsystem exhibits modal characteristics similar to those of the linear subsystem corresponding to the non-linear one in the neighbourhood of the point of the static equilibrium. In this study, the natural frequencies and the natural periods of the BT subsystem, equal to respective natural frequencies and natural periods of the above-defined linear subsystem, are introduced.

Service velocities at which forced resonances in the BTT system may occur, commonly called the critical/resonant service velocities (the static pressures of the moving wheel sets induce a cyclic excitation of the bridge), can be predicted. The $\bar{T}_i = T_j$ forced resonance occurs at the resonant velocity calculated from the approximate formula (PN-82/S-10052 1982)

$$v = v_{ij} = \frac{j^2}{i} L_v f_1 \ , \quad i,j = 1,2,\dots \tag{15}$$

where: $\bar{T}_i$ - period of i-th harmonic of the cyclic excitation, T_j - j-th natural period of the BT subsystem, $L_v = 24.78$ m - length of the ICE-3 rail-vehicle. The fundamental natural frequency of BT subsystem equals $f_1 = 1/T_1$. The fundamental natural period of the BT subsystem is estimated from the formula $T_1 = s/v$, where: s - distance of the moving load head per one cycle of free damped vibrations. Periods of subsequent harmonics of the quasi-static excitation of the bridge-track subsystem are as follows

$$\bar{T}_i = \frac{L_v}{iv} \ , i = 1,2,\dots. \tag{16}$$

Based on the preliminary simulations, the resonant speeds are slightly lower (ca. by 3%) compared to the values obtained from Eqn. (15) due to the effect of parametric excitation induced by moving wheel sets.

8. Numerical analyses of BTT systems

Vibrations of the BTT systems are transient processes that may tend to quasi steady-state processes at selected resonant service velocities. The resonant processes may be interfered/amplified by several factors specific to the BTT systems, i.e., structural complexity, fast-varying configuration, potential micro-separations and re-contacts/impacts of moving wheel-sets, limited number of moving rail-vehicles, random track irregularities.

Random samples of vertical track irregularities are calculated using the Monte-Carlo method, according to Eqs. (2-3). Taking into account the stationary and ergodic Gaussian model of the track irregularities as well as a physically non-linear BTT model, it is hypothesized that the analysed quantities are approximately random continuous variables described by respective normal distributions cut on both sides. This hypothesis is verified numerically in this Section.

An n-element simple random sample of quantity Z is considered. The basic statistics (expectance $E(Z)$ and standard deviation $D(Z)$) of an n-element sample of

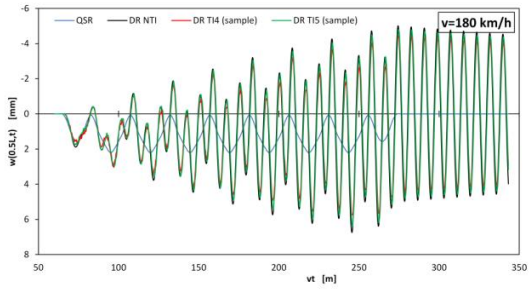

Fig. 8 SCB-15 bridge (RSE). Output quantity $w(0.5L,t)$ [mm] for resonant service velocity $v_{31} = 180$ km/h

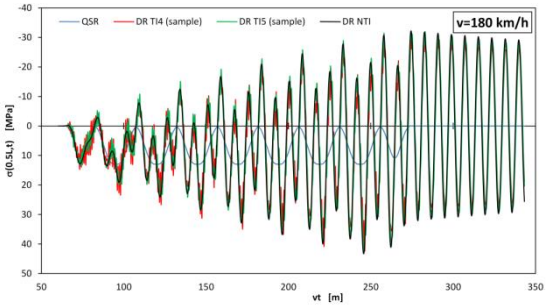

Fig. 9 SCB-15 bridge (RSE). Output quantity $\sigma(0.5L,t)$ [MPa] for resonant service velocity $v_{31} = 180$ km/h

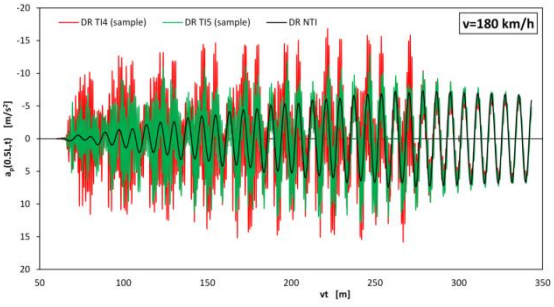

Fig. 10 SCB-15 bridge (RSE). Output quantity $a_p(0.5L,t)$ [m/s^2] before low pass filtering, for resonant service velocity $v_{31} = 180$ km/h

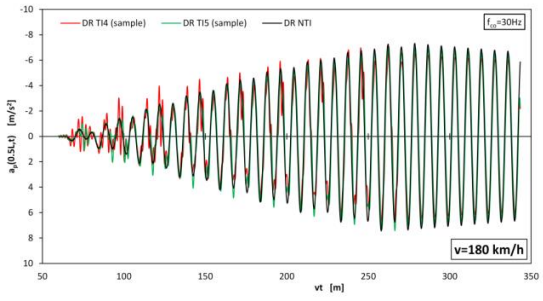

Fig. 11 SCB-15 bridge (RSE). Output quantity $a_p(0.5L,t)$ [m/s^2] after low pass filtering ($f_{co} = 30$ Hz), for resonant service velocity $v_{31} = 180$ km/h

quantity Z are calculated using well-known classic formulae. In this study, eight quantities defined in Section 4 are analysed, i.e., $w_{\max}$, $\sigma_{\max}$, $a_{p,\max}^{\mathrm{LPF}}$, $R_{\min}$,

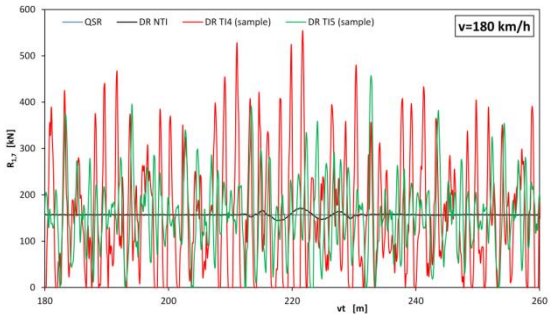

Fig. 12 SCB-15 bridge (RSE). Output quantity $R_{1,7}(t)$ [kN] for resonant service velocity$v_{31} = 180$ km/h

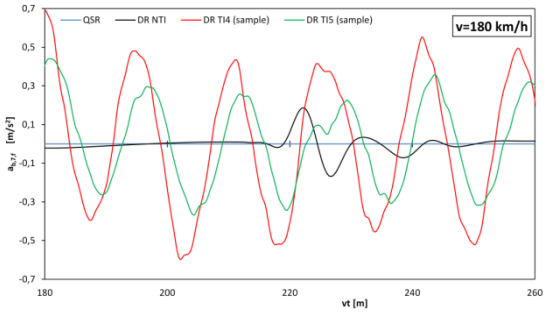

Fig. 13 SCB-15 bridge (RSE). Output quantity $a_{b.7.f}(t)$ [m/s^2] for resonant service velocity $v_{31} = 180$ km/h

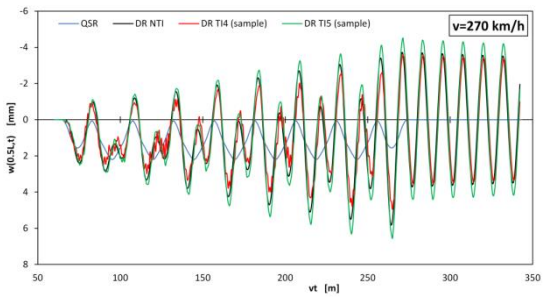

Fig. 14 SCB-15 bridge (RSE). Output quantity $w(0.5L,t)$ [mm] for resonant service velocity $v_{21} = 270$ km/h

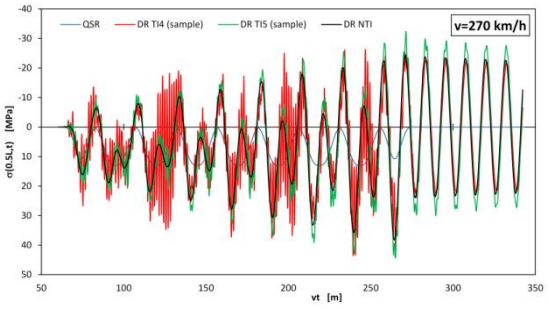

Fig. 15 SCB-15 bridge (RSE). Output quantity $\sigma(0.5L,t)$ [MPa] for resonant service velocity $v_{21} = 270$ km/h

$a_{\mathrm{b,max}}$, $\varphi_w(0.5L)$, $\varphi_\sigma(0.5L)$, $\sigma_f(0.5L)$.

Numerical dynamic analyses are conducted for five bridges forming the SCB series described in Section 2, using the corresponding computer code worked out in the Delphi language in (Podworna and Klasztorny 2014c).

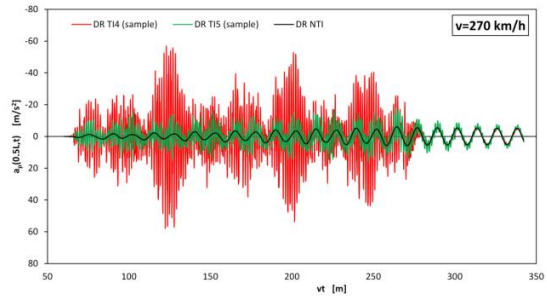

Fig. 16 SCB-15 bridge (RSE). Output quantity $a_p(0.5L,t)$ [m/s^2] before low pass filtering, for resonant service velocity $v_{21} = 270$ km/h

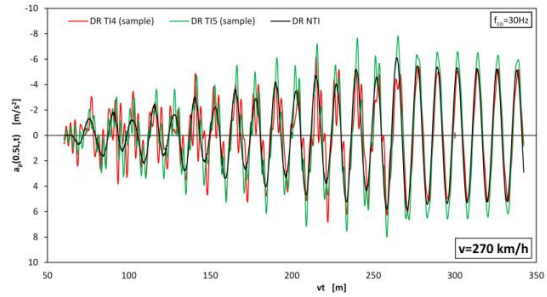

Fig. 17 SCB-15 bridge (RSE). Output quantity $a_p(0.5L,t)$ [m/s^2] after low pass filtering ($f_{co} = 30$ Hz), for resonant service velocity $v_{21} = 270$ km/h

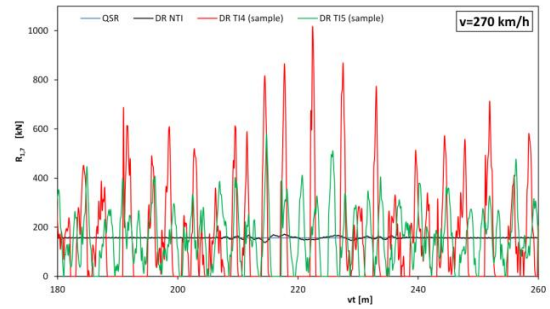

Fig. 18 SCB-15 bridge (RSE). Output quantity $R_{1,7}(t)$ [kN] for resonant service velocity $v_{21} = 270$ km/h

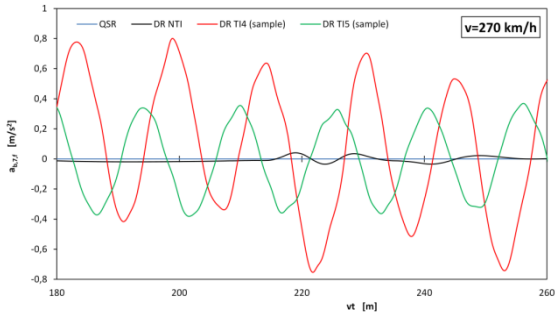

Fig. 19 SCB-15 bridge (RSE). Output quantity $a_{b.7.f}(t)$ [m/s^2] for resonant service velocity $v_{21} = 270$ km/h

A time step h=2×10^{-5} sec for numerical integration of the equations of motion (14) was determined with high accuracy in (Podworna and Klasztorny 2014c) and provides the output functions with good accuracy.

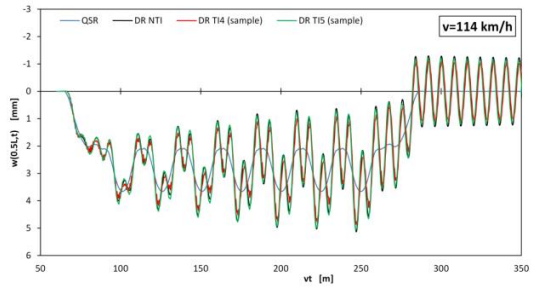

Fig. 20 SCB-27 bridge (RSE). Output quantity $w(0.5L,t)$ [mm] for resonant service velocity $v_{31} = 114$ km/h

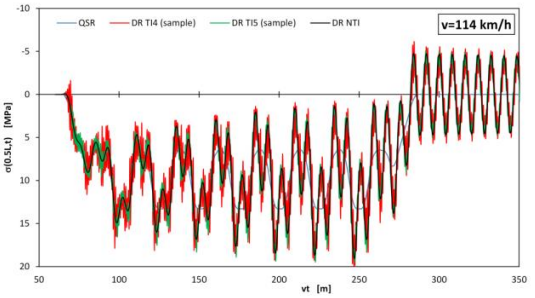

Fig. 21 SCB-27 bridge (RSE). Output quantity $\sigma(0.5L,t)$ [MPa] for resonant service velocity $v_{31} = 114$ km/h

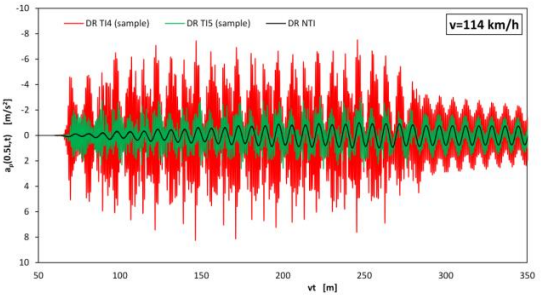

Fig. 22 SCB-27 bridge (RSE). Output quantity $a_p(0.5L,t)$ [m/s^2] before low pass filtering, for resonant service velocity $v_{31} = 114$ km/h

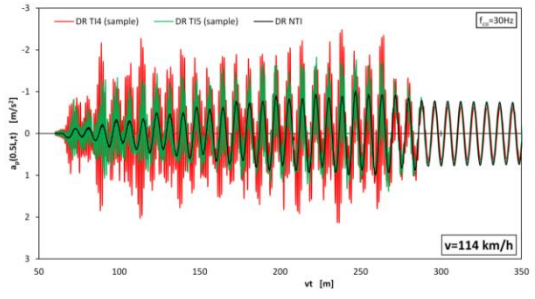

Fig. 23 SCB-27 bridge (RSE). Output quantity $a_p(0.5L,t)$ [m/s^2] after low pass filtering ($f_{co} = 30$ Hz), for resonant service velocity $v_{31} = 114$ km/h

8.1 The time-histories of output quantities

The following codes are introduced: QSR - quasi-static response, DR - dynamic response, RSE - random simulation example, NTI-no track irregularities, TI4, TI5, TI6- random

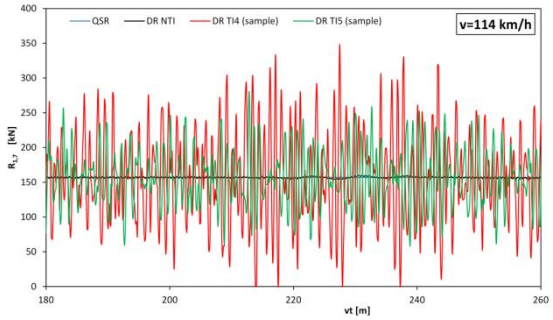

Fig. 24 SCB-27 bridge (RSE). Output quantity $R_{1,7}(t)$ [kN] for resonant service velocity $v_{31} = 114$ km/h

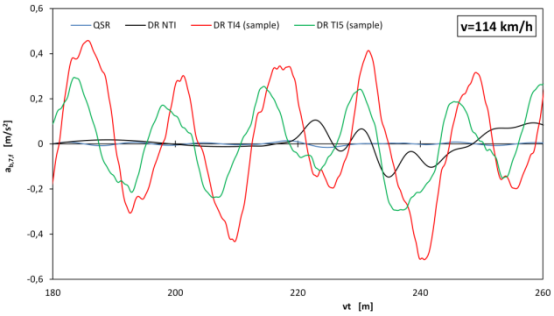

Fig. 25 SCB-27 bridge (RSE). Output quantity $a_{b.7.f}(t)$ [m/s^2] for resonant service velocity $v_{31} = 114$ km/h

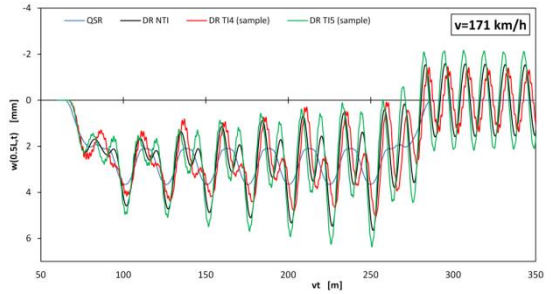

Fig. 26 SCB-27 bridge (RSE). Output quantity $w(0.5L,t)$ [mm] for resonant service velocity $v_{21} = 171$ km/h

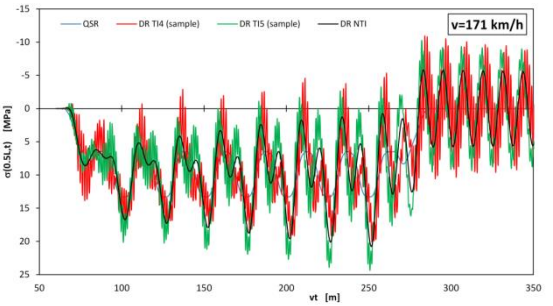

Fig. 27 SCB-27 bridge (RSE). Output quantity $\sigma(0.5L,t)$ [MPa] for resonant service velocity $v_{21} = 171$ km/h

track irregularities corresponding to line grades LG = 4, 5, 6, respectively. The dynamic time-histories of the selected quantities, corresponding to the most dangerous resonant speeds of the ICE-3 train, are shown in Figs. 8-19 for the shortest bridge (SCB-15), and in Figs. 20-31 for the longest

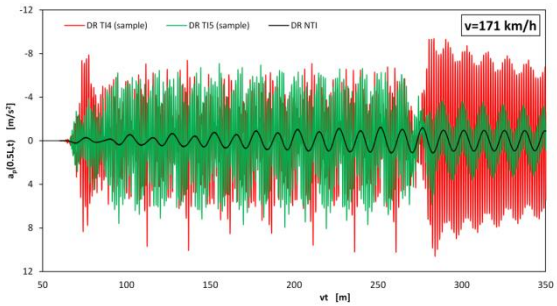

Fig. 28 SCB-27 bridge (RSE). Output quantity $a_p(0.5L,t)$ [m/s^2] before low pass filtering, for resonant service velocity $v_{21} = 171$ km/h

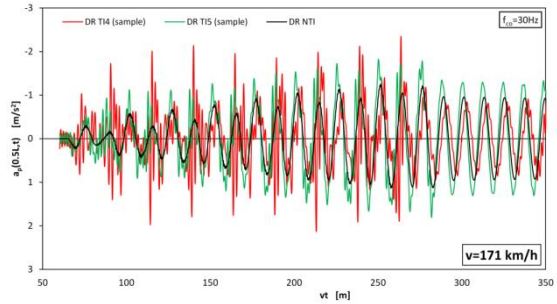

Fig. 29 SCB-27 bridge (RSE). Output quantity $a_p(0.5L,t)$ [m/s^2] after low pass filtering ($f_{co} = 30$ Hz), for resonant service velocity $v_{21} = 171$ km/h

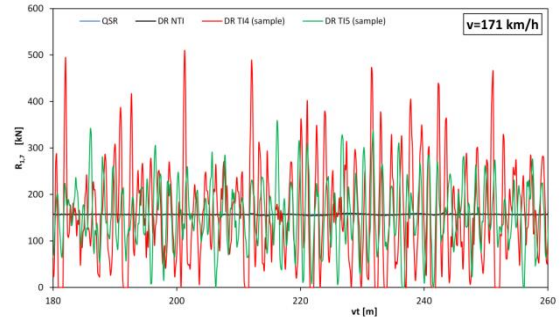

Fig. 30 SCB-27 bridge (RSE). Output quantity $R_{1,7}(t)$ [kN] for resonant service velocity $v_{21} = 171$ km/h

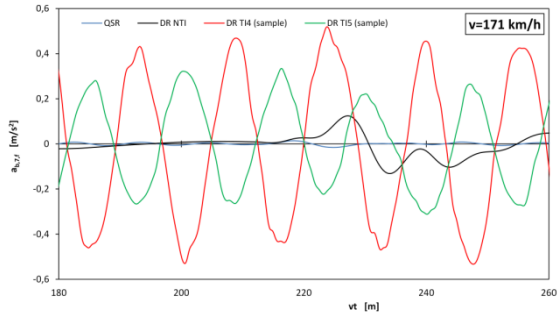

Fig. 31 SCB-27 bridge (RSE). Output quantity $a_{b.7.f}(t)$ [m/s^2] for resonant service velocity $v_{21} = 171$ km/h

one (SCB-27). The results shown in Figs. 8-13, corresponding to the train velocity of $v = 180$ km/h, are cited from (Podworna and Klasztorny 2014c) for

comparative purposes. Random time-histories correspond to randomly selected samples of track irregularities TI4 and TI5. Random time-histories of the vertical displacement at midspan, $w(0.5L,t)$, the normal stress in the bottom fibres of the main steel beams, $\sigma(0.5L,t)$, are shown in a background of the quasi-static response (QSR) and the dynamic response for a smooth track (DR NTI).

The excitation of the SCB-15 bridge vibrations has a periodic pulsating mode and acts in a short period of time (Fig. 8). When the train enters the bridge at the speed of $v_{31} = 180$ km/h, the bridge deflection oscillates with a quasi-linearly increasing amplitude; the oscillation amplification is observed with the predicted frequency (Fig. 8). The impact of track irregularities TI4 and TI5 on the bridge deflection is small (Fig. 8).

The dynamic response of the SCB-15 bridge in stress at the speed of $v_{31} = 180$ km/h is similar to the response of deflection, however, there appear high-frequency oscillations of small amplitudes, superimposed on the main oscillations (Fig. 9). The influence of the track irregularities TI4 and TI5 on the normal stress in the main steel beams is small (Fig. 9).

Time-histories of vertical accelerations of the SCB-15 bridge deck at the train speed $v_{31} = 180$ km/h are affected by high-frequency oscillations caused by track irregularities (Fig. 10). In the case of TI4 irregularities, the acceleration amplitudes increase more than twice compared with the smooth track (Fig. 10). It should be noted that the limit acceleration $a_{p,u} = 5$ m/s^2 is exceeded even in the case of the smooth track because of the resonant amplification (Fig. 10). After low pass filtering with cut-off frequency 30 Hz according to (PN-EN1990 2004), the impact of irregularities TI4 and TI5 on the acceleration $a_p(0.5L,t)$ is small (Fig. 11).

The non-linear model of wheel-rail contact, used in this study, allows the simulation of non-linear wheelset-track interactions, including micro-detachment and pulse impact of the wheel sets on the rail. Time-histories of the interaction force with the largest amplitudes (the first wheel set in the seventh vehicle) corresponding to the irregularities TI4 and TI5 are shown in Fig. 12. In the case of TI4 track irregularities (the alert limit defined in (PN-EN13848-5 2010)), there are multiple micro-separations of the wheel set and the wheel set dynamic pressure often exceeding the static pressure twice (Fig. 12). In the case of TI5 irregularities, the wheel set dynamic pressure is much smaller and micro-separations are rare (Fig. 12). This is the second time the phenomenon has been presented since the previous approaches did not allow for their identification (double-sided wheel-rail constraints, no contact stiffness and/or modal superposition method). In addition, an experimental technology capable of measuring the wheel-rail interaction forces has not been developed, yet.

The micro-separations and impulses of wheel sets induced by the track irregularities do not affect significantly the vehicle-body acceleration time-histories (Fig. 13). In the case of the SCB-15 bridge and the resonant speed of $v_{31} = 180$ km/h the passenger comfort is maintained at a very good level, even in the case of irregularities corresponding to the alert limit (PN-EN13848-5 2010).

In the case of the SCB-15 bridge and the smooth track the resonant speed $v_{31} = 180$ km/h leads to higher vibrations than the speed $v_{21} = 270$ km/h (Figs. 8 and 14). The influence of the track irregularities on the bridge deflection at the speed v_{21} amounts to ca. ± 10% (Fig. 14). The high-frequency oscillations of small amplitudes are visible (Fig. 14).

The impact of TI4 track irregularities on the stress time-histories in the SCB-15 bridge, at the resonant speed $v_{21} = 270$ km/h can be significant and manifests high-frequency oscillations with big amplitudes (Fig. 15). The effect of high-frequency oscillation truncation due to operation of only 2000 output points is observed in the graphs (Fig. 15). However, the extreme values analysed in further considerations were determined automatically by a computer programme taking into account all the numerical integration points of the equations of motion.

High-frequency oscillations with big amplitudes are evident also in the vertical acceleration of the SCB-15 bridge deck, at the resonant speed $v_{21} = 270$ km/h (Fig. 16). After filtration of these oscillations in accordance with (PN-EN1990 2004), there are obtained the time-histories compatible with the curve for the smooth track, in which the amplitudes of the extra oscillations overlapping the main time-histories exceed 3.5 m/s^2 (Fig. 17).

Time-histories of the interaction $R_{1,7}(t)$, corresponding to the SCB-15 bridge with track irregularities TI4 and TI5 and the speed of 270 km/h (Fig. 18), maps the micro-separations of the wheel set from the track and the multiple impacts of the moving wheel set of the pulses greater than for the speed of 180 km/h (Fig. 12). In the case of TI4 track irregularities, the wheel-set dynamic pressure exceeds the static pressure even a few times, which indicates that TI4 irregularities are unacceptable at this speed (Fig. 18). The passenger comfort criterion for the train speed of 270 km/h and the track with irregularities is satisfied at a very good level (Figs. 13 and 19).

Dynamic effects in the longest bridge, SCB-27, both with and without the track irregularities (Figs. 20-31) are much smaller than those in the shortest bridge, SCB-15 (Figs. 8-19). This is due to the excitation which is oscillatory but with a small amplitude and a substantial constant component (Figs. 20 and 26). The resonance effect in deflection and stress of the SCB-27 bridge, at the resonance speed $v_{31} = 114$ km/h, is small (Figs. 20 and 21). The stress graphs demonstrate the high-frequency oscillations of small amplitudes (Fig. 21).

The vertical accelerations of the SCB-27 bridge platform at the speed v_{31} are relatively small, and after filtering do not exceed 3 m/s^2 (Figs. 22 and 23). Micro-separations of the first wheel set in the seventh vehicle are intermittent in the case of TI4 irregularities and do not appear in the case of TI5 irregularities (Fig. 24). The derailment risk in the case of TI5 irregularities is low (Fig. 24). The passenger comfort is at a very good level both in the case of TI5 and TI4 irregularities (Fig. 25).

In the case of the SCB-27 bridge and the speed $v_{21} = 171$ km/h, the dynamic effects are significant (Figs. 26 - 28, and 30). Track irregularities TI4 and TI5 cause changes in the deflection amplitudes of about ±15%. The

Table 3 Random values of design quantities for BTT=SCB-15/T/ICE-3 system corresponding to selected random track irregularities (RSE)

v [km/h]	TI	$w_{\max}$ [mm]	$\sigma_{\max}$ [MPa]	$a_{p,\max}^{LPF}$ [m/s^2]	$R_{\min}$ [kN]	$a_{b,\max}$ [m/s^2]
30	NTI	2.2	13.0	~0	156.4	~0
v_{31}=180	NTI	6.7	43.3	7.4	141.4	0.2
v_{31}=180	TI6	6.9	44.8	7.3	49.9	0.4
v_{31}=180	TI5	6.4	42.1	7.0	0	0.7
v_{31}=180	TI4	5.8	42.4	6.9	0	1.1
v_{21} = 270	NTI	5.8	38.3	6.1	136.5	0.2
v_{21} = 270	TI6	6.0	40.0	6.3	21.2	0.4
v_{21} = 270	TI5	6.6	44.4	7.3	0	0.6
v_{21} = 270	TI4	5.0	43.6	6.7	0	1.1
$v_{\max}$=300	NTI	4.4	27.2	3.8	138.7	0.1
$v_{\max}$=300	TI6	4.3	27.5	3.9	0	0.2
$v_{\max}$=300	TI5	4.3	29.3	4.2	0	0.4
$v_{\max}$=300	TI4	4.2	33.8	4.0	0	0.7

Table 4 Random values of design quantities for BTT=SCB-18/T/ICE-3 system corresponding to selected random track irregularities (RSE)

v [km/h]	TI	$w_{\max}$ [mm]	$\sigma_{\max}$ [MPa]	$a_{p,\max}^{LPF}$ [m/s^2]	$R_{\min}$ [kN]	$a_{b,\max}$ [m/s^2]
30	NTI	2.9	14.1	~0	156.3	~0
v_{31}=149	NTI	5.8	29.4	3.0	150.6	0.2
v_{31}=149	TI6	5.6	28.5	3.2	98.8	0.3
v_{31}=149	TI5	5.3	29.1	3.7	0	0.5
v_{31}=149	TI4	7.0	37.4	4.8	0	0.9
v_{21}=225	NTI	2.9	15.2	0.9	145.7	0.1
v_{21}=225	TI6	3.3	19.2	1.0	13.1	0.4
v_{21}=225	TI5	4.0	24.2	1.3	0	0.8
v_{21}=225	TI4	4.9	30.6	1.9	0	1.1
$v_{\max}$=300	NTI	5.3	26.6	2.6	140.6	0.2
$v_{\max}$=300	TI6	5.3	29.5	3.4	7.2	0.3
$v_{\max}$=300	TI5	5.0	32.3	3.8	0	0.5
$v_{\max}$=300	TI4	6.3	38.2	4.3	0	1.0

Table 5 Random values of design quantities for BTT=SCB-21/T/ICE-3 system corresponding to selected random track irregularities (RSE)

v	TI	$w_{\max}$ [mm]	$\sigma_{\max}$ [MPa]	$a_{p,\max}^{LPF}$ [m/s^2]	$R_{\min}$ [kN]	$a_{b,\max}$ [m/s^2]
30	NTI	3.2	14.0	~0	156.3	~0
v_{31}=135	NTI	3.8	17.2	0.8	154.6	0.1
v_{31}=135	TI6	3.6	17.5	1.0	93.0	0.2
v_{31}=135	TI5	4.4	20.9	1.5	6.2	0.5
v_{31}=135	TI4	4.3	23.5	2.7	0	0.8
v_{21}=203	NTI	5.4	24.3	1.9	150.4	0.2
v_{21}=203	TI6	5.2	24.8	2.2	34.7	0.4
v_{21}=203	TI5	6.6	31.4	2.4	0	0.8
v_{21}=203	TI4	7.0	36.1	3.8	0	1.1
$v_{\max}$=300	NTI	5.9	26.0	2.6	141.4	0.2
$v_{\max}$=300	TI6	6.3	28.6	2.8	2.0	0.4
$v_{\max}$=300	TI5	6.5	37.1	3.7	0	0.5
$v_{\max}$=300	TI4	6.6	37.8	4.6	0	0.9

Table 6 Random values of design quantities for BTT=SCB-24/T/ICE-3 system corresponding to selected random track irregularities (RSE)

v	TI	$w_{\max}$ [mm]	$\sigma_{\max}$ [MPa]	$a_{p,\max}^{LPF}$ [m/s^2]	$R_{\min}$ [kN]	$a_{b,\max}$ [m/s^2]
30	NTI	3.5	13.7	~0	156.3	~0
v_{21}=185	NTI	6.4	25.6	2.1	151.9	0.3
v_{21}=185	TI6	6.8	29.0	2.2	46.5	0.5
v_{21}=185	TI5	6.4	28.6	2.6	0	0.7
v_{21}=185	TI4	5.7	29.3	3.0	0	1.2
v_{31}=123	NTI	6.5	25.9	2.2	149.9	0.3
v_{31}=123	TI6	6.6	26.8	2.3	106.8	0.4
v_{31}=123	TI5	6.1	25.5	2.4	23.3	0.5
v_{31}=123	TI4	7.3	29.9	2.8	0	0.7
$v_{\max}$=300	NTI	7.1	27.9	2.6	143.7	0.3
$v_{\max}$=300	TI6	6.7	28.2	3.3	0	0.3
$v_{\max}$=300	TI5	7.5	31.1	4.2	0	0.7
$v_{\max}$=300	TI4	7.8	37.6	4.9	0	0.9

Table 7 Random values of design quantities for BTT=SCB-27/T/ICE-3 system corresponding to selected random track irregularities (RSE)

v	TI	$w_{\max}$ [mm]	$\sigma_{\max}$ [MPa]	$a_{p,\max}^{LPF}$ [m/s^2]	$R_{\min}$ [kN]	$a_{b,\max}$ [m/s^2]
30	NTI	3.7	13.3	~0	156.4	~0
v_{21}=171	NTI	5.6	20.8	1.3	153.2	0.2
v_{21}=171	TI6	5.8	22.4	1.4	71.3	0.3
v_{21}=171	TI5	6.4	24.4	1.8	0	0.7
v_{21}=171	TI4	5.1	20.1	2.3	0	0.8
v_{31}=141	NTI	5.1	19.0	1.0	153.0	0.2
v_{31}=141	TI6	5.1	19.3	1.1	111.1	0.3
v_{31}=141	TI5	5.1	19.6	1.8	34.5	0.4
v_{31}=141	TI4	4.9	19.9	2.1	0	0.7
$v_{\max}$=300	NTI	7.7	28.2	2.7	145.5	0.3
$v_{\max}$=300	TI6	5.8	22.4	3.1	71.3	0.3
$v_{\max}$=300	TI5	8.8	39.8	3.4	0	0.7
$v_{\max}$=300	TI4	9.3	41.0	4.8	0	0.8

Table 8 System BTT=SCB-15/T/ICE-3 with track irregularities TI4, TI5. Basic statistics of design quantities for resonant speeds

Quantity	TI	v_{21}=270				v_{31}=180			
		$w_{\max}$ [mm]	$\sigma_{\max}$ [MPa]	$a_{p,\max}^{LPF}$ [m/s^2]	$a_{b,\max}$ [m/s^2]	$w_{\max}$ [mm]	$\sigma_{\max}$ [MPa]	$a_{p,\max}^{LPF}$ [m/s^2]	$a_{b,\max}$ [m/s^2]
Z	NTI	5.8	38.3	6.1	0.2	6.7	43.3	7.4	0.2
Z_l	TI4	4.2	29.2	5.8	0.8	3.0	22.4	6.8	0.9
Z_u	TI4	8.2	56.7	6.7	1.1	10.8	73.0	8.2	1.1
$E(Z)$	TI4	6.1	44.5	6.2	0.9	6.9	47.8	7.5	1.0
$D(Z)$	TI4	1.1	7.9	0.3	0.1	2.1	14.0	0.4	0.1
Z_l	TI5	4.4	31.2	4.8	0.5	5.0	34.3	7.0	0.5
Z_u	TI5	7.1	47.8	7.6	0.7	9.3	59.5	7.8	0.8
$E(Z)$	TI5	5.8	40.7	6.3	0.6	7.2	47.6	7.5	0.7
$D(Z)$	TI5	0.8	5.1	0.7	0.1	1.2	7.3	0.3	0.1

Table 9 System BTT=SCB-18/T/ICE-3 with track irregularities TI4, TI5. Basic statistics of design quantities for resonant speeds

Quantity	TI	v_{21}=225				v_{31}=149			
		$w_{\max}$ [mm]	$\sigma_{\max}$ [MPa]	$a_{p,\max}^{LPF}$ [m/s^2]	$a_{b,\max}$ [m/s^2]	$w_{\max}$ [mm]	$\sigma_{\max}$ [MPa]	$a_{p,\max}^{LPF}$ [m/s^2]	$a_{b,\max}$ [m/s^2]
Z	NTI	2.9	15.24	0.9	0.1	5.8	29.4	3.0	0.2
Z_l	TI4	4.2	26.5	0.8	1.1	4.0	24.2	2.4	0.7
Z_u	TI4	5.5	34.6	2.1	1.5	7.6	39.2	5.0	0.9
$E(Z)$	TI4	4.8	30.4	1.4	1.2	5.6	30.8	3.8	0.8
$D(Z)$	TI4	0.3	1.9	0.4	0.1	0.9	4.2	0.7	0.1
Z_l	TI5	3.8	20.9	0.8	0.7	4.8	25.5	2.4	0.5
Z_u	TI5	4.1	25.1	1.4	0.8	6.7	36.1	4.1	0.7
$E(Z)$	TI5	4.0	23.4	1.1	0.8	5.8	30.9	3.3	0.5
$D(Z)$	TI5	0.1	1.2	0.2	0.1	0.6	3.0	0.5	0.1

Table 10 System BTT=SCB-21/T/ICE-3 with track irregularities TI4, TI5. Basic statistics of design quantities for resonant speeds

Quantity	TI	v_{21}=203				v_{31}=135			
		$w_{\max}$ [mm]	$\sigma_{\max}$ [MPa]	$a_{p,\max}^{LPF}$ [m/s^2]	$a_{b,\max}$ [m/s^2]	$w_{\max}$ [mm]	$\sigma_{\max}$ [MPa]	$a_{p,\max}^{LPF}$ [m/s^2]	$a_{b,\max}$ [m/s^2]
Z	NTI	5.4	24.3	1.9	0.2	3.8	17.2	0.8	0.1
Z_l	TI4	3.6	21.8	1.6	1.0	3.7	18.9	0.6	0.7
Z_u	TI4	7.5	39.3	4.2	1.3	5.1	27.1	3.0	0.8
$E(Z)$	TI4	5.9	30.7	2.6	1.2	4.5	23.8	1.7	0.7
$D(Z)$	TI4	1.1	4.7	0.6	0.1	0.4	2.4	0.7	0.0
Z_l	TI5	4.1	20.7	1.8	0.2	3.5	17.5	0.7	0.4
Z_u	TI5	6.6	33.3	2.4	0.7	4.3	21.9	1.8	0.5
$E(Z)$	TI5	5.7	28.2	2.0	0.9	3.9	19.4	1.2	0.4
$D(Z)$	TI5	0.8	3.6	0.2	0.8	0.3	1.3	0.3	0.0

Table 11 System BTT=SCB-24/T/ICE-3 with track irregularities TI4, TI5. Basic statistics of design quantities for resonant speeds

Quantity	TI	v_{21}=185				v_{31}=123			
		$w_{\max}$ [mm]	$\sigma_{\max}$ [MPa]	$a_{p,\max}^{LPF}$ [m/s^2]	$a_{b,\max}$ [m/s^2]	$w_{\max}$ [mm]	$\sigma_{\max}$ [MPa]	$a_{p,\max}^{LPF}$ [m/s^2]	$a_{b,\max}$ [m/s^2]
Z	NTI	6.4	25.6	2.1	0.3	6.5	25.9	2.2	0.3
Z_l	TI4	5.3	25.8	1.7	0.9	5.8	24.1	1.9	0.6
Z_u	TI4	8.3	40.4	3.3	1.3	7.2	32.3	3.0	0.9
$E(Z)$	TI4	7.1	33.0	2.4	1.1	6.6	28.4	2.3	0.7
$D(Z)$	TI4	0.9	3.9	0.6	0.1	0.5	2.1	0.3	0.1
Z_l	TI5	5.7	24.8	1.8	0.7	6.0	25.1	2.0	0.4
Z_u	TI5	7.7	35.0	2.8	0.8	6.9	29.4	2.5	0.7
$E(Z)$	TI5	6.6	30.6	2.3	0.7	6.5	27.2	2.3	0.5
$D(Z)$	TI5	0.6	2.8	0.4	0.1	0.3	1.2	0.1	0.1

Table 12 System BTT=SCB-27/T/ICE-3 with track irregularities TI4, TI5. Basic statistics of design quantities for resonant speeds

Quantity	TI	v_{21}=171				v_{31}=141			
		$w_{\max}$ [mm]	$\sigma_{\max}$ [MPa]	$a_{p,\max}^{LPF}$ [m/s^2]	$a_{b,\max}$ [m/s^2]	$w_{\max}$ [mm]	$\sigma_{\max}$ [MPa]	$a_{p,\max}^{LPF}$ [m/s^2]	$a_{b,\max}$ [m/s^2]
Z	NTI	5.7	20.8	1.3	0.3	5.1	19.1	1.0	0.2
Z_l	TI4	4.5	21.0	1.0	0.8	4.7	18.2	0.7	0.5
Z_u	TI4	7.3	34.9	2.7	1.2	5.6	22.3	2.5	0.9
$E(Z)$	TI4	6.4	28.2	1.3	1.0	5.2	21.0	1.4	0.7
$D(Z)$	TI4	0.8	3.9	0.8	0.1	0.3	1.1	0.7	0.1
Z_l	TI5	4.8	19.0	1.0	0.6	4.9	18.7	0.8	0.4
Z_u	TI5	6.7	29.0	2.1	0.8	5.4	21.2	2.3	0.6
$E(Z)$	TI5	5.7	23.3	1.4	0.7	5.1	20.1	1.4	0.4
$D(Z)$	TI5	0.6	2.9	0.3	0.1	0.2	0.6	0.5	0.0

charts of normal stress $\sigma(0.5L,t)$ disclose high-frequency oscillations of the medium amplitudes (Fig. 27).

Vertical accelerations of the SCB-27 bridge platform at a speed of 171 km/h are relatively small, and, after filtration of the high-frequency oscillations, slightly exceed 2 m/s^2 (Figs. 28-29). The derailment risk increases at the velocity $v_{21} = 171$ km/h compared with the velocity of $v_{31} = 114$ km/h (Figs. 24 and 30). The passenger comfort is ensured at a very good level in all the analysed cases (Fig. 31).

8.2 The results of the design quantities

The values of the design quantities, corresponding to the SCB series of bridges with selected random track irregularity samples, are summarized in Tables 3-7. The most dangerous resonant service velocities v_{31}, v_{21} for the subsequent bridge spans and the maximum velocity $v_{\max} = 300$ km/h are taken into consideration.

Table 3 presents the random values of the design quantities for BTT=SCB-15/T/ICE-3 system (the shortest bridge span), corresponding to selected random track irregularities TI4 (the alert limit (PN-EN1990 20904)), TI5 and TI6 (a nearly smooth track). The deterministic values corresponding to the smooth track, in both static and dynamic conditions, are presented as well. In the resonance states the maximum dynamic deflection exceeds the static deflection even three times. The track irregularities may increase or decrease the maximum dynamic deflection to ~10%. For the maximum speed of the train the maximum dynamic deflection is greater twice compared to the maximum static deflection. Deflections of the bridge are many times smaller than the limit value $w_u = L/600 = 25$ mm.

The maximum static normal stress in the bottom of the main beams of the BTT=SCB-15/T/ICE-3 system, induced by an ICE-3 train, does not exceed 9% of the limit value. The maximum dynamic stress may even be 3.5 times greater than the corresponding static value. Track irregularities may increase or decrease the maximum stress up to ~15%. The biggest effort occurs at the resonant service speed of v_{31}. The traffic safety criterion is unsatisfied.

For the smooth track in the BTT=SCB-15/T/ICE-3 system, the derailment risk is very low. In the resonant states, micro-separations of the wheel-sets from the track do not occur only for very small track irregularities (TI6). Micro-detachment exists in all the cases for medium (TI5)

and large (TI4) track irregularities (high risk the train derailment). The passenger comfort criterion is satisfied in all the cases undertaken, at a very good level.

Though not identical, similar results are also obtained for the 18, 21, 24 and 27 span bridges. The results are collected in Tables 4-7.

Tables 4-7 collect the random values of the design quantities for BTT systems, corresponding to selected random track irregularities TI4, TI5 and TI6. The deterministic values corresponding to the smooth track, in both static and dynamic conditions, are also presented. At the resonant velocity v_{21} no resonance effect is observed for the smooth track, and for the TI4 track irregularities the maximum dynamic deflection increases the static deflection by 70% for the SCB-18, by ~ 2 times for the SCB-21,24,27 objects. The track irregularities may increase or decrease the maximum dynamic deflection to ~20%, 30%, 12%, 45% for SCB-18, 21, 24, 27 respectively. Vertical deflections at the bridge midspans are many times smaller than the limit values (30 mm, 35 mm, 40 mm, 45 mm respectively).

The maximum static normal stress in the bottom fibres of the main beams of the superstructures, induced by an ICE-3 train, does not exceed 9% of the limit value. The maximum dynamic stress may be ~ 2 times greater than the corresponding static value. Track irregularities may increase or decrease the maximum stress even twice. The traffic safety criterion is met at the resonance speeds and the maximum service speeds but in the BTT=SCB-18/T/ICE-3 system only for track irregularities TI5 and TI6.

For the smooth track in the BTT systems the derailment risk is very low. In the resonant states micro-separations of the wheel-sets from the track do not occur only for very small track irregularities (TI6). Micro-detachment exists in all the cases for medium (TI5) and large (TI4) track irregularities (high risk of derailment of the train). The passenger comfort criterion is fulfilled at a very good or good level in all the cases undertaken.

8.3 The statistical analysis

The basic statistics of the design quantities, in reference to the SCB bridges loaded by an ICE-3 train moving at resonant service velocities v_{21}, v_{31} , taking into consideration track irregularities TI4 and TI5, are listed in Tables 8-12. The statistics are calculated for 20-element random sample sets. The deterministic results corresponding to the smooth track (NTI) are also included. In each table, the lowest (Z_l) and the highest (Z_u) random values of quantity Z are given as well as the expectance $E(Z)$ and the standard deviation $D(Z)$.

The results given in Tables 8-12 confirm the hypothesis that the output quantities $w_{\max}$, $\sigma_{\max}$, $a_{p,\max}^{\mathrm{LPF}}$, $a_{\mathrm{b,max}}$ behave approximately as continuous random variables with the normal distribution cut-off symmetrically on both sides. As expected, the ranges of variation of these quantities are generally smaller for TI5 irregularities compared with TI4 irregularities. There is no regular relationship of the parameters of these variables vs. a span length or a resonance operating speed. The calculations were performed using the values with higher accuracy than those in Tables 8-12.

Each random variable in Tables 8-12 is characterized by the following parameters:

- increase of the expectance relative to the deterministic value: $(E - Z)/Z \times 100\%$;
- the range of variation up: $(Z_u - E)/E \times 100\%$;
- the range of variation down: $(E - Z_l)/E \times 100\%$;
- relative standard deviation: $D/E \times 100\%$.

For the maximum vertical deflection $w_{\max}$ one obtains:

- increase of the expectance:
  (-3)-60% for TI4 and 0-40% for TI5;
- the range of variation up:
  5-60% for TI4 and 5-30% for TI5;
- the range of variation down:
  5-60% for TI4 and 5-30% for TI5;
- relative standard deviation:
  2-30% for TI4 and 2-20% for TI5.

For the maximum normal stress $\sigma_{\max}$ one obtains:

- increase of the expectance:
  5-100% for TI4 and 5-40% for TI5;
- the range of variation up:
  5-55% for TI4 and 5-30% for TI5;
- the range of variation down:
  5-55% for TI4 and 5-30% for TI5;
- relative standard deviation:
  2-30% for TI4 and 3-15% for TI5.

For the maximum acceleration of bridge decks after filtering, $a_{p,\max}^{\mathrm{LPF}}$, one obtains:

- increase of the expectance:
  0-40% for TI4 and 0-40% for TI5;
- the range of variation up:
  5-95% for TI4 and 4-50% for TI5;
- the range of variation down:
  5-90% for TI4 and 4-40% for TI5;
- relative standard deviation:
  3-60% for TI4 and 2-25% for TI5.

For the maximum vertical acceleration of vehicle bodies, $a_{b,\max}$, one obtains:

- increase of the expectance:
  300-1200% for TI4 and 200-800% for TI5;
- the range of variation up:
  10-30% for TI4 and 15-50% for TI5;
- the range of variation down:
  10-30% for TI4 and 15-50% for TI5;
- relative standard deviation:
  6-15% for TI4 and 7-30% for TI5.

8.4 The results of impact factors

Table 13 collects the values of impact factors $\varphi_w(0.5L), \varphi_\sigma(0.5L)$ calculated for respective Z_u and tests for the ultimate limit state criterion with fatigue for TI4 and TI5 track irregularities samples (RSE). The top estimation is adopted in the following form

$$\begin{aligned} \sigma_m(0.5L) &= \beta \max_t \sigma_s(0.5L, t) \\ \sigma_a(0.5L) &= \sigma_{max} - \sigma_m(0.5L) \end{aligned} \tag{17}$$

where $\beta = 0.50,\ 0.51,\ 0.63,\ 0.70,\ 0.74$ for SCB-15, SCB-18, SCB-21, SCB-24, SCB-27, respectively. The values of parameter β are based on the static and dynamic

Table 13 Values of impact factors and ultimate limit state criterion test for BTT systems with track irregularities TI4 and TI5

SCB	v [km/h]	TI	$\varphi_w(0.5L)$	$\varphi_\sigma(0.5L)$	$\sigma_a(0.5L)$ [MPa]	$\sigma_f(0.5L)$ [MPa]
SCB-15	180	TI4	4.9	5.6	66.5	196.1
SCB-15	270	TI4	3.7	4.4	50.2	157.9
SCB-15	300	TI4	2.5	3.4	38.1	129.9
SCB-15	180	TI5	4.2	4.6	53.0	164.6
SCB-15	270	TI5	3.2	3.7	41.3	137.0
SCB-15	300	TI5	2.2	2.9	30.9	112.5
SCB-18	149	TI4	2.6	2.8	32.0	119.3
SCB-18	225	TI4	1.9	2.5	27.4	108.3
SCB-18	300	TI4	2.3	3.1	37.0	130.9
SCB-18	149	TI5	2.3	2.6	28.9	112.0
SCB-18	225	TI5	1.4	1.8	17.9	86.0
SCB-18	300	TI5	2.1	2.6	30.1	114.8
SCB-21	135	TI4	1.6	1.9	18.3	91.7
SCB-21	203	TI4	2.3	2.8	30.5	120.2
SCB-21	300	TI4	2.5	3.6	41.3	145.8
SCB-21	135	TI5	1.4	1.6	13.1	79.4
SCB-21	203	TI5	2.1	2.4	24.4	106.1
SCB-21	300	TI5	2.2	2.8	30.2	119.7
SCB-24	123	TI4	2.1	2.4	22.8	105.7
SCB-24	185	TI4	2.4	3.0	30.8	124.7
SCB-24	300	TI4	2.7	3.7	41.2	149.1
SCB-24	123	TI5	2.0	2.2	19.8	98.8
SCB-24	185	TI5	2.2	2.6	25.5	112.2
SCB-24	300	TI5	2.4	3.3	35.5	135.7
SCB-27	114	TI4	1.5	1.7	12.5	81.9
SCB-27	171	TI4	2.0	2.6	25.0	111.3
SCB-27	300	TI4	2.8	3.9	42.5	152.4
SCB-27	114	TI5	1.4	1.4	8.8	73.3
SCB-27	171	TI5	1.8	2.2	19.2	97.6
SCB-27	300	TI5	2.4	3.6	38.5	143.1

normal stress time-histories in the bottom fibres of the main steel beams at the resonant speeds of the train (Figs. 9, 15, 21, 27). Static normal stress σ_{gk}, induced by self-weight of the bridges, is 33.47 MPa, 36.78 MPa, 39.84 MPa, 42.71 MPa, 44.95 MPa for the subsequent bridges.

On the basis of the content of Table 13, the following conclusions can be drawn:

- The impact factors $\varphi_w(0.5L)$, $\varphi_\sigma(0.5L)$ do not increase monotonically as the train speed increases.
- In general, the impact factors $\varphi_w(0.5L)$, $\varphi_\sigma(0.5L)$ do not depend on a bridge span except for the shortest bridge span (SCB-15) and the resonance speed $v_{31} = 180$ km/h (the values of these factors are much higher than those in other SCB bridges).
- The values of $\varphi_\sigma(0.5L)$ are greater than the corresponding values of $\varphi_w(0.5L)$ by 0-50% and, most typically, by ~ 35%.
- The values of $\varphi_w(0.5L)$, corresponding to the TI4 irregularities, are higher by 5-36%, compared to the respective values for TI5 irregularities. Generally, the increase is ~15%.
- The values of $\varphi_\sigma(0.5L)$, corresponding to the TI4 irregularities, are higher by 8-40%, compared to the respective values for TI5 irregularities. Generally, the increase is ~20%.
- The ultimate limit state criterion with high-cyclic fatigue is met for the bridges SCB-18, SCB-21, SCB-24, SCB-27 in terms of the resonance speeds and the maximum speed as well as of TI4 and TI5 track irregularities. Only in the SCB-15 bridge the effective stresses $\sigma_f(0.5L)$ exceed the limit stress $\sigma_u = 157$ MPa in the case of resonant speeds and TI4 irregularities and in the case of the resonant speed $v_{31} = 180$ km/h and TI5 irregularities.

9. Conclusions

The conclusions are related to the vertical vibrations of the SCB bridges, the ballasted track and an ICE-3 train.

- The bridges forming the SCB series, traversed by a high-speed ICE-3 train moving on the ballasted track, are physically non-linear complex systems and their dynamic response can be determined only numerically. The simulations are needed in a wide range of the operating speed.
- The serviceability limit state criterion expressed in terms of the vertical deflection of a bridge superstructure is met in all the cases studied (smooth track NTI; track irregularities TI4, TI5, TI6; train speed up to 300 km/h). In the reference cases of the resonant speeds and the smooth track, vibration amplitudes of the bridge superstructures increase quasi-linearly. Track irregularities mostly disturb the deflection time-histories by an additional increase or detuning.
- The ultimate limit state criterion with high-cyclic fatigue is met for bridges SCB-18, SCB-21, SCB-24, SCB-27 in terms of the resonance speeds and the maximum speed as well as of TI4, TI5, and TI6 track irregularities. Only in the SCB-15 bridge the effective stresses $\sigma_f(0.5L)$ exceed the limit stress $\sigma_u = 157$ MPa in the case of resonant speeds and TI4 irregularities and in the case of the resonant speed $v_{31} = 180$ km/h and TI5 irregularities. Therefore, there should be imposed appropriate limitations on operating speeds depending on the track condition.
- The traffic safety criterion is met for SCB-18, SCB-21, SCB-24, SCB-27 bridges. Only for SCB-15 bridge this criterion is not satisfied for some resonant speeds and the smooth track or the track with irregularities.
- The passenger comfort condition is satisfied almost in all the cases studied.
- For the smooth track, there is no micro-detachments of wheel-sets from the rails. The maximum unloading of wheel sets is 2-11% depending on the bridge span length and the operating speed.
- In the cases of the resonant service speeds and TI4/TI5 track irregularities, there can occur multiple micro-separations of the wheel sets from the rails and multiple wheel-rail impacts. This can lead to high dynamic

pressures of the wheel-sets onto the track. The dynamic pressures decrease as the span length increases or the line grade increases. This phenomenon requires an experimental verification and a further study using more advanced contact models.

• At the resonant operating speeds, random vertical track irregularities may cause detuning or increase the resonant effects in the SCB bridges.

The railway bridges forming the SCB series, loaded by an ICE-3 high-speed train moving on the ballasted track with track irregularities of line grades LG=4, 5, 6, conform to the required design conditions excluding the SCB-15 bridge.

Acknowledgements

This work was supported by the National Centre for Science, Poland, as a part of project No. N N506 0992 40, realized in the period 2011-2013. This support is gratefully acknowledged. The author would like to express many thanks to Professor Marian Klasztorny for his valuable remarks and suggestions.

References

Antolin, P., Zhang, N., Goicolea, J.M., Xia, H., Astiz, M.A. and Oliva, J. (2013), "Consideration of nonlinear wheel-rail contact forces for dynamic vehicle-bridge interaction in high-speed railways", *J. Sound Vib*., **332**, 1231-1251.

Au, F.T.K., Wang, J.J. and Cheung, Y.K. (2002), "Impact study of cable stayed railway bridges with random rail irregularities", *Eng. Struct.*, **24**, 529-541.

Cheng, Y.S., Au, F.T.K. and Cheung, Y.K. (2001), "Vibration of railway bridges under a moving train by using bridge-track-vehicle element", *Eng. Struct*., **23**(12), 1597-1606.

Doménech, A.P., Museros, P. and Martínez-Rodrigo, M.D. (2014), "Influence of the vehicle model on the prediction of the maximum bending response of simply-supported bridges under high-speed railway traffic", *Eng. Struct*., **72**, 123-139.

Fryba, L. (1996), *Dynamics of Railway Bridges*, Academia, Praha.

Fryba, L. (2001), "A rough assessment of railway bridges for high speed trains", *Eng. Struct.*, **23**, 548-556.

Guo, W.W., Xia, H., De Roeck, G. and Liu, K. (2012), "Integral model for train-track-bridge interaction on the Sesia viaduct: Dynamic simulation and critical assessment", *Comput. Struct.*, **112-113**, 205-216.

http (2010a), www.siemens.com/mobility.

http (2010b), www.db-baureihen.de/br/fernverkehr/403.php.

http (2010c), www.hochgeschwindigkeitszuege.com/germany/index_ice_3.htm.

Lei, X. and Noda, N.A. (2002) "Analyses of dynamic response of vehicle and track coupling system with random irregularity of track vertical profile", *J. Sound Vib*., **258(**1), 147-165.

Lu, F., Lin, J.H., Kennedy, D. and Williams, F.W. (2009), "An algorithm to study non-stationary random vibrations of vehicle - bridge system", *Comput. Struct.*, **87**, 177-185.

PN-82/S-10052 (1982), Bridge objects, Steel structures, Design. (in Polish)

PN-85/S-10030 (1985), Bridge objects, Loads. (in Polish)

PN-EN13848-5 (2010), Eurocode: Railway applications-Track-Track geometry quality-Part 5: Geometric quality levels-Plain line.

PN-EN1990 (2004), Eurocode: Basis of structural design/Annex A1: Application for bridges (National Annex, Poland).

Podworna, M. (2005), "Vertical vibrations of steel beam bridges induced by trains moving at high speeds. Part 1-theory", *Arch. Civil Eng.*, **51** (2), 179-209.

Podworna, M. (2005), "Vertical vibrations of steel beam bridges induced by trains moving at high speeds. Part 2 - numerical analysis", *Arch. Civil Eng*., **51**(2), 211-231.

Podworna, M. and Klasztorny, M. (2014), "Vertical vibrations of composite bridge / track structure / high-speed train system. Part 2: Physical and mathematical modelling", *Bull. Polish Acad. Sci. Tech. Sci.*, **62**(1), 191-196.

Podworna, M. and Klasztorny, M. (2014), "Vertical vibrations of composite bridge / track structure / high-speed train system. Part 3: Deterministic and random vibrations of exemplary system", *Bull. Polish Acad. Sci. Tech. Sci.*, **62**(2), 305-320.

Podworna, M. and Klasztorny, M., (2014) "Vertical vibrations of composite bridge / track structure / high-speed train system. Part 1: Series-of-types of steel-concrete bridges", *Bull. Polish Acad. Sci. Tech. Sci.*, **62**(1), 165-179.

Rocha, J.M., Henriques, A.A. and Calcada, R. (2014), "Probabilistic safety assessment of a short span high-speed railway bridge", *Eng. Struct.*, **71**, 99-111.

Song, M.K. and Choi, C.K. (2002), "Analysis of high-speed vehicle-bridge interactions by a simplified 3-D model", *Struct. Eng. Mech.*, **13(**5), 505-532.

Song, M.K., Noh, H.C. and Choi, C.K. (2003), "A new three dimensional finite element analysis model of high-speed train-bridge interactions", *Eng. Struct.*, **25**, 1611-1626.

Steimel, A. (2007), *Electric Traction - Motion Power and Energy Supply: Basics and Practical Experience*, Oldenbourg Industrieverlag GmbH.

Wiriyachai, A., Chu, K.H. and Gang, V.K. (1982), "Bridge impact due to wheel and track irregularities", *ASCE J. Eng. Mech. Div.*, **108**(4), 648-666.

Zhang, N., Xia, H. and Guo, W. (2008), "Vehicle-bridge interaction analysis under high-speed trains", *J. Sound Vib.*, **309**, 407-425.

CC